Cellular and Molecular Mechanisms of Atrial Arrhythmogenesis in Patients with Paroxysmal Atrial Fibrillation

Supplemental Material

Niels Voigt, MD*, Jordi Heijman, PhD*, Qiongling Wang, PhD, David Y. Chiang, BSc, Na Li, PhD, Matthias Karck, MD, Xander H.T. Wehrens, MD, PhD, Stanley Nattel, MD, and Dobromir Dobrev, MD

* These authors contributed equally to this work

Corresponding Author:
Dobromir Dobrev, MD
Hufelandstrasse 55
45122 Essen
Phone: 0049 201 723 3477
Fax: 0049 201 723 5593
E-Mail: Dobromir.Dobrev@uk-essen.de

Contents

Patient Characteristics

Right-atrial appendages were dissected from sinus rhythm (Ctl) patients and paroxysmal AF (pAF) patients (defined as patients with normal sinus rhythm during the operation but at least one documented self-terminating AF episode lasting less than 7 days, **Online Figure I**) undergoing open-heart surgery (**Online-Tables I-III**). Experimental protocols were approved by the Medical Faculty Mannheim, University of Heidelberg (No. 2011–216N-MA). Each patient gave written informed consent.

Online Table I: Characteristics of patients used for functional studies

	Ctl	pAF
Patients, n	35	17
Gender, m/f	28/7	12/5
Age, y	69.2±1.4	71.5±1.4
Body mass index, kg/m^2	28.0±1.0	29.0±1.4
CAD, n	21	11
MVD/AVD, n	7	5
CAD+MVD/AVD, n	7	1
Hypertension, n	32	16
Diabetes, n	13	6
Hyperlipidemia, n	23	11
LAD, mm	42.6±1.1	42.4±1.2
LVEF, %	50.3±2.1	47.9±4.5
Time since last AF episode, days; median (range)	-	10 (1-58)
Digitalis, n	2	3
ACE inhibitors, n	22	10
AT1 blockers, n	5	2
β-Blockers, n	26	13
Dihydropyridines, n	6	4
Diuretics, n	12	8
Nitrates, n	5	4
Lipid-lowering drugs, n	24	13

Values are presented as mean±SEM, median (range), or number of patients. CAD, coronary artery disease; LAD, left atrial diameter, MVD/AVD, mitral/aortic valve disease; LVEF, left ventricular ejection fraction; ACE, angiotensin-converting enzyme; AT, angiotensin receptor.

Online Table II: Characteristics of patients used to determine Ca^{2+}-handling parameters in voltage-clamp experiments

	Ctl	pAF
Patients, n	25	9
Gender, m/f	21/4	8/1
Age, y	69.5±1.9	73.8±1.5
Body mass index, kg/m^2	27.1±0.9	30.3±2.1
CAD, n	16	4
MVD/AVD, n	5	4
CAD+MVD/AVD, n	4	1
Hypertension, n	22	9
Diabetes, n	9	1
Hyperlipidemia, n	16	7
LAD, mm	42.7±1.3	43.6±1.1
LVEF, %	52.2±2.4	47.4±8.3
Time since last AF episode, days; median (range)	-	20 (3-58)
Digitalis, n	0	1
ACE inhibitors, n	16	7
AT1 blockers, n	3	0
β-Blockers, n	18	7
Dihydropyridines, n	5	2
Diuretics, n	8	6
Nitrates, n	3	1
Lipid-lowering drugs, n	17	7

Values are presented as mean±SEM, median (range), or number of patients. CAD, coronary artery disease; MVD/AVD, mitral/aortic valve disease; LAD, left atrial diameter; LVEF, left ventricular ejection fraction; ACE, angiotensin-converting enzyme; AT, angiotensin receptor.

Online Table III: Characteristics of patients used for biochemistry

	Ctl	pAF
Patients, n	40	32
Gender, m/f	30/10	22/10
Age, y	67.3±1.5	70.3±1.8
Body mass index, kg/m^2	28.2±0.7	28.3±1.1
CAD, n	19	13
MVD/AVD, n	11	10
CAD+MVD/AVD, n	10	9
Hypertension, n	36	28
Diabetes, n	12	10
Hyperlipidemia, n	32	22
LAD, mm	40.9±0.8	43.0±1.0
LVEF, %	57.0±1.8	52.2±2.3
Time since last AF episode, days; median (range)	-	18 (1-72)
Digitalis, n	1	5
ACE inhibitors, n	29	22
AT1 blockers, n	4	4
β-Blockers, n	25	23
Dihydropyridines, n	11	7
Diuretics, n	13	17
Nitrates, n	4	5
Lipid-lowering drugs, n	24	20

Values are presented as mean±SEM, median (range), or number of patients. CAD, coronary artery disease; MVD/AVD, mitral/aortic valve disease; LAD, left atrial diameter; LVEF, left ventricular ejection fraction; ACE, angiotensin-converting enzyme; AT, angiotensin receptor.

Experimental Methods

1. Measurement of Intracellular [Ca^{2+}] and Patch-clamp Experiments

Intracellular [Ca^{2+}] was quantified using Fluo-3-acetoxymethyl ester (Fluo-3 AM; Invitrogen, Carlsbad, CA; 10 µmol/L, 10 min loading and 30 min de-esterification).[1] Simultaneously, membrane currents or -potentials were recorded in whole-cell ruptured-patch configuration using voltage-clamp or current-clamp techniques, respectively. Borosilicate glass microelectrodes had tip resistances of 2-5 MΩ when filled with pipette solution, containing (in mmol/L): EGTA 0.02, Fluo-3 0.1 (Invitrogen), GTP-Tris 0.1, HEPES 10, K-aspartate 92, KCl 48, Mg-ATP 1, Na_2-ATP 4; pH=7.2. Seal-resistances were 4-8 GΩ. For voltage-clamp experiments series resistance and cell capacitance were compensated.

During experiments, myocytes were superfused at 37°C with a bath solution containing (in mmol/L): $CaCl_2$ 2, glucose 10, HEPES 10, KCl 4, $MgCl_2$ 1, NaCl 140, probenecid 2; pH=7.4. For voltage-clamp experiments, K$^+$-currents were blocked by adding 4-aminopyridine (5 mmol/L) and $BaCl_2$ (0.1 mmol/L) to the bath solution. pClamp-Software (V10.2, Molecular Devices, Sunnyvale, CA) was used for data acquisition and analysis. Drugs were applied via a rapid solution exchange system (ALA Scientific Instruments, Long Island, NY). Caffeine (10 mmol/L) was used for rapid depletion and quantification of SR Ca^{2+}-content.[2]

L-type Ca^{2+}-currents ($I_{Ca,L}$) were activated at a rate of 0.5 Hz in voltage-clamp configuration using the following protocol: starting from a holding-potential of -80 mV, fast Na$^+$-currents were inactivated using a 100-ms ramp-pulse to -40 mV. A consecutive 100-ms depolarizing step to +10 mV activated $I_{Ca,L}$, which triggered corresponding [Ca^{2+}]$_i$-transients (CaTs). Action potentials were triggered in current-clamp configuration using 1 ms current pulses of 1.2x threshold strength applied at 0.5 Hz.

2. Quantification of Serca2a Activity

Ca^{2+}-reuptake into the SR mediated by SR Ca^{2+}-ATPase (Serca2a) and Ca^{2+} extrusion into extracellular space by Na$^+$/Ca^{2+} exchanger (NCX1, forward-mode) are the major contributors to the decay of $I_{Ca,L}$-induced Ca^{2+}-transient (CaT).[3] This decay is commonly described with a mono-exponential equation:

$$[\mathrm{Ca}^{2+}]_\mathrm{i}(\mathrm{t}) = \left([\mathrm{Ca}^{2+}]_\mathrm{Amplitude} \times \exp\left(-\mathrm{k}_\mathrm{syst} \times \mathrm{t}\right)\right) + [\mathrm{Ca}^{2+}]_\mathrm{diast}$$

where $[\mathrm{Ca}^{2+}]_\mathrm{i}(\mathrm{t})$, $[\mathrm{Ca}^{2+}]_\mathrm{Amplitude}$ *and* $[\mathrm{Ca}^{2+}]_\mathrm{diast}$ represent the Ca^{2+} concentration at the timepoint *t,* the CaT amplitude and the diastolic Ca^{2+} level, respectively. The rate constant of decay k_syst largely reflects the rate of combined Ca^{2+} transport by Serca and NCX and may therefore be expressed as the sum of the two separate rate constants:

$$\mathrm{k}_\mathrm{syst} = \mathrm{k}_\mathrm{Serca} + \mathrm{k}_\mathrm{NCX}$$

Since, the decay of caffeine-induced CaT (cCaT) is almost exclusively due to Ca^{2+} removal via NCX, k_{NCX} can be estimated by analysing the rate of decay of the cCaT (k_{caff}):

$$k_{caff} \approx k_{NCX}$$

Using this approach Serca activity can be estimated by:

$$k_{Serca} = k_{syst} - k_{caff}$$

3. Quantification of Diastolic SR Ca^{2+}-Leak with Tetracaine

SR Ca^{2+}-leak in intact human atrial myocytes was measured according to Shannon et al.[4] using Na^{+}- and Ca^{2+}-free bath solution (containing, in mmol/L: 4-aminopyridine 5, $BaCl_2$ 0.1, EGTA 10, glucose 10, HEPES 10, KCl 4, $LiCl_2$ 140, Mg_2Cl 1, probenecid 2) and tetracaine (1 mmol/L).

4. Immunoblot Analysis

The protein levels of calsequestrin (CSQ, 1:2500; Dianova, Hamburg, Germany), NCX1 (1:1000; Fitzgerald, Concord, MA); total RyR2 (1:500, Affinity BioReagents, Golden, CO), Ser2808- and Ser2814-phosphorylated RyR2 (1:2000 and 1:1000, respectively),[5, 6] Serca2a (1:2000, Santa Cruz Biotechnology, Santa Cruz, CA), total, Ser16- and Thr17-phosphorylated phospholamban (PLB; all 1:5000, Badrilla Ltd., Leeds, United Kingdom), catalytic PKA-subunit (PKAc, 1:1000; BD Biosciences, Franklin Lakes, NJ); regulatory $PKA_{II\alpha}$-subunit ($PKA_{II\alpha}$, 1:500, Santa Cruz Biotechnology), calmodulin (1:1000; abcam, Cambridge, UK), total CaMKIIδ (1:200; Santa Cruz Biotechnology, Santa Cruz, CA), Thr287-phosphorylated CaMKIIδ (1:5000; Promega, Madison, WI), catalytic PP1α-subunit (1:500; Biomol, Plymouth Meeting, Pa), and total catalytic PP2A (1:1000, affinity purified; Upstate Biotechnology, Lake Placid, NY), were quantified by Western blotting as described previously.[7, 8] The Ser2808-RyR2 and Ser2814-RyR2 phospho-epitope-specific antibodies were custom generated using the peptide C-RTRRI-(pS)-QTSQV corresponding to the PKA phosphorylation site region at Ser2808 on RyR2 and peptide CSQTSQV-(pS)-VD corresponding to CaMKII phosphorylated RyR2 at Ser2814.

Appropriate peroxidase-conjugated goat anti-rabbit (Sigma-Aldrich) and goat anti-mouse (Sigma-Aldrich) were used as secondary antibodies and visualized by chemifluorescense (GE Healthcare, Chalifont St. Giles, UK). Chemiluminescence was quantified using a LAS1000 chemiluminescence detection system (FujiFilm, Düsseldorf, Germany) and AIDA software (Raytest, Sprockhövel, Germany). Protein expression was normalized to CSQ, which was unchanged in paroxysmal AF compared to sinus rhythm (Ctl) samples (**Online Figure III**), in agreement with previous findings.[9]

5. Preparation of Sarcoplasmic-reticulum (SR) Fractions

Atrial tissues were homogenized on ice in a solution containing 10 mM HEPES, 500 mM sucrose and 5 mM EDTA supplemented with 20 mM NaF, 1 mM Na_3VO_4, and protease inhibitor and phosphatase inhibitor cocktails (cOmplete, Mini and PhosSTOP from Roche Applied Science, Indianapolis, IN). The homogenates were then subjected to three sequential steps of centrifugation. First, the homogenates were centrifuged at 3,800 g for 15 min at 4°C. Second, the supernatants were collected and centrifuged at 27,900 g for 15 min at 4°C. Third, the supernatants were ultracentrifuged at 110,000 g for 1 hour at 4°C. The supernatants were removed and the pellets resuspended in 50 µl of the same solution as for homogenization but without the EDTA. The resultant suspensions were used for single channel recording and Western blot analysis.

6. Quantification of RyR2 Expression and Phosphorylation in SR-fractions

Sarcoplasmic reticulum preparations were incubated with 2x Laemmli Sample Buffer (Bio-Rad, Hercules, CA) at room temperature for 30 min before being subjected to electrophoresis on 5 and 10% stacked acrylamide gels, and transferred onto polyvinyl difluoride membranes overnight at 4°C. Antibodies against the following targets were used to probe the membranes: RyR2 (MA3-916; Thermo Fisher Scientific, Waltham, MA), RyR2 pS2808 (custom), RyR2 pS2814 (custom), and calsequestrin (CSQ; PA1-913; Thermo Fisher Scientific). Membranes were then incubated with secondary anti-mouse and anti-rabbit antibodies conjugated respectively to Alexa-Fluor 680 (Molecular Probes, Eugene, OR) and IR800Dye (Rockland Immunochemicals, Gilbertsville, PA). Bands were quantified using Image J.

7. RyR2 Single-channel Recordings

Single-channel recordings of ryanodine-receptor channels (cardiac subtype; RyR2) were obtained under voltage-clamp conditions at 0 mV, as previously described.[10] Atrial SR membrane-preparations were incorporated into lipid-bilayer membranes comprised of a mixture of phosphatidylethanolamine and phosphatidylserine at a 3:1 ratio (Avanti Polar Lipids, Alabaster, AL) dissolved in n-decane (25 mg/ml). Bilayers were formed across a 150 µm aperture of a polystyrene cuvette. The *trans* chamber (corresponding to the luminal side of the SR) contained (in mmol/L) HEPES 250, KCl 50 and $Ca(OH)_2$ 53. The *cis* chamber (corresponding to the cytosolic side of the SR) contained (in mmol/L) HEPES 250, Tris-base 125, KCl 50, EGTA 1, $CaCl_2$ 0.5, pH=7.35. Ryanodine (5 µmol/L) was applied to the *cis* chamber to confirm identity of RyR2 channels at the end of each experiment. Data were collected using Digidata 1322A (Molecular Devices, Sunnyvale, CA) and Warner Bilayer Clamp Amplifier BC-535 (Warner Instruments, Hamden, CT) under voltage-clamp conditions. Cytosolic free [Ca^{2+}] was calculated with WinMax32. Data were analyzed from digitized current recordings using pCLAMP-9.2 software (Molecular Devices).

Definition of Computational Model

1. Ca^{2+}-buffers and Simulation of EGTA

The Ca^{2+}-buffers in the cytosol (low-affinity troponin-C sites, high-affinity Ca^{2+} and Mg^{2+} troponin-C sites, calmodulin, myosin, and SR-membrane sites), in the SR (calsequestrin) and in the subsarcolemmal compartments (low- and high-affinity sarcolemmal binding sites) were incorporated into every Ca^{2+}-domain *d* of each segment *s* based on their first-order implementation in the model by Grandi et al.[11] Unless specified otherwise, all simulations were performed with normal, intact (non-Ca^{2+}-buffered) Ca^{2+} handling ($[\mathrm{EGTA}]_{\mathrm{max}} = 0\ \mathrm{mmol/L}$). In order to reproduce experiments performed in the presence of EGTA in the pipette solution, we included EGTA as a potential Ca^{2+}-buffer in a subset of simulations. EGTA was included as a Ca^{2+}-buffer in the cytosolic and subsarcolemmal compartments with a maximum concentration identical to that specified in the experimental conditions and with first-order on and off rates based on the work of Smith et al:[12]

$$\frac{\mathrm{d[EGTA]_{bound,cyt}}}{\mathrm{dt}} = \mathrm{k_{on,EGTA}} \times [\mathrm{Ca^{2+}}]_{\mathrm{cyt}}^{\mathrm{s,d}} \times \left([\mathrm{EGTA}]_{\mathrm{max}} - [\mathrm{EGTA}]_{\mathrm{bound,cyt}}\right) \\ - \mathrm{k_{off,EGTA}} \times [\mathrm{EGTA}]_{\mathrm{bound,cyt}}$$

$$\mathrm{k_{on,EGTA}} = 5.0\ (\mathrm{mmol/L})^{-1}\mathrm{ms}^{-1}, \qquad \mathrm{k_{off,EGTA}} = 7.5 \cdot 10^{-4}\ \mathrm{ms}^{-1}$$

$$\mathrm{J_{Buff,Ca,cyt}^{s,b}} = \frac{\mathrm{d[TnC_{low}]_{bound}}}{\mathrm{dt}} + \frac{\mathrm{d\left[TnC_{high,Ca}\right]_{bound}}}{\mathrm{dt}} + \frac{\mathrm{d\left[TnC_{high,Mg}\right]_{bound}}}{\mathrm{dt}} + \frac{\mathrm{d[CaM]_{bound}}}{\mathrm{dt}} \\ + \frac{\mathrm{d[Myosin_{Ca}]_{bound}}}{\mathrm{dt}} + \frac{\mathrm{d\left[Myosin_{Mg}\right]_{bound}}}{\mathrm{dt}} + \frac{\mathrm{d[SR_{buff}]_{bound}}}{\mathrm{dt}} + \frac{\mathrm{d[EGTA]_{bound,cyt}}}{\mathrm{dt}}$$

2. Model Structure

2.1. Cellular Compartmentation

The virtual model cell was divided into 50 longitudinal segments ($\mathrm{N_{Seg}} = 50$). Each segment contains two membrane domains (including subsarcolemmal space) with all transmembrane ion channels, and 18 subcellular Ca^{2+}-domains ($\mathrm{N_{Dom}} = 18$). Each domain contains a cytosolic space, sarcoplasmic reticulum (SR), and SR Ca^{2+}-release space (SRS; representing a microdomain around the SR in which neighboring ryanodine receptor (RyR2) channels can activate each other. In addition to RyR2 channels, each Ca^{2+}-domain contains formulations for SR Ca^{2+}-uptake by a Serca2a/PLB complex.

The volume of each subcellular compartment was similar to that in Grandi et al.,[11] with the volume of the newly introduced SRS compartment set at 0.1% of cell volume:

$$\mathrm{v_{cell}} = 33\ \mathrm{pL}$$

$$\mathrm{v_{cyt}} = 0.65 \times \mathrm{v_{cell}}, \qquad \mathrm{v_{SR}} = 0.035 \times \mathrm{v_{cell}}$$

$$\mathrm{v_{SRS}} = 0.001 \times \mathrm{v_{cell}}, \qquad \mathrm{v_{subsl}} = 0.02 \times \mathrm{v_{cell}}$$

2.2. Ca^{2+}-Diffusion

For every segment *s*, Ca^{2+} can diffuse from a given Ca^{2+}-domain *d* to its left neighbor *d-1* and its right neighbor *d+1* (**Figure 7A**). This diffusion is implemented for all three compartments (albeit with different diffusion rates). The left subsarcolemmal space is considered the left neighbor of Ca^{2+}-domain 0 (the leftmost domain). Similarly, the right subsarcolemmal space is considered the right neighbor of Ca^{2+}-domain 17 (the rightmost domain). The diffusion between segments occurs similarly, with Ca^{2+} diffusing from segment *s*, domain *d* to domain *d* in segments *s-1* and segment *s+1*.

For every segment *s* (between 0 and 49, inclusive) and domain *d* (between 0 and 17, inclusive), Ca^{2+} diffusion is then determined as follows (with $[\mathrm{Ca}^{2+}]_{\mathrm{X}}^{-1,\mathrm{d}} = [\mathrm{Ca}^{2+}]_{\mathrm{X}}^{0,\mathrm{d}}$, $[\mathrm{Ca}^{2+}]_{\mathrm{X}}^{50,\mathrm{d}} = [\mathrm{Ca}^{2+}]_{\mathrm{X}}^{49,\mathrm{d}}$, $[\mathrm{Ca}^{2+}]_{\mathrm{X}}^{\mathrm{s},-1} = [\mathrm{Ca}^{2+}]_{\mathrm{X}}^{\mathrm{s},0}$, and $[\mathrm{Ca}^{2+}]_{\mathrm{X}}^{\mathrm{s},18} = [\mathrm{Ca}^{2+}]_{\mathrm{X}}^{\mathrm{s},17}$ for all three compartments):

$$\tau_{\mathrm{diff,dom,cyt}} = 0.60\ \mathrm{ms}, \qquad \tau_{\mathrm{diff,seg,cyt}} = \tau_{\mathrm{diff,dom,cyt}}$$

$$\tau_{\mathrm{diff,dom,SR}} = 15\ \mathrm{ms}, \qquad \tau_{\mathrm{diff,seg,SR}} = \tau_{\mathrm{diff,dom,SR}}$$

$$\tau_{\mathrm{diff,dom,SRS}} = 0.125\ \mathrm{ms}, \qquad \tau_{\mathrm{diff,seg,SRS}} = 0.30\ \mathrm{ms}$$

$$\tau_{\mathrm{diff,SRS\leftrightarrow cyt}} = 12\ \mathrm{ms}$$

$$\begin{aligned}\mathrm{J}_{\mathrm{diff,cyt}}^{\mathrm{s,d}} = {} & \left([\mathrm{Ca}^{2+}]_{\mathrm{cyt}}^{\mathrm{s,d-1}} + [\mathrm{Ca}^{2+}]_{\mathrm{cyt}}^{\mathrm{s,d+1}} - 2 \times [\mathrm{Ca}^{2+}]_{\mathrm{cyt}}^{\mathrm{s,d}}\right) / \tau_{\mathrm{diff,dom,cyt}} \\ & + \left([\mathrm{Ca}^{2+}]_{\mathrm{cyt}}^{\mathrm{s-1,d}} + [\mathrm{Ca}^{2+}]_{\mathrm{cyt}}^{\mathrm{s+1,d}} - 2 \times [\mathrm{Ca}^{2+}]_{\mathrm{cyt}}^{\mathrm{s,d}}\right) / \tau_{\mathrm{diff,seg,cyt}}\end{aligned}$$

$$\begin{aligned}\mathrm{J}_{\mathrm{diff,SR}}^{\mathrm{s,d}} = {} & \left([\mathrm{Ca}^{2+}]_{\mathrm{SR}}^{\mathrm{s,d-1}} + [\mathrm{Ca}^{2+}]_{\mathrm{SR}}^{\mathrm{s,d+1}} - 2 \times [\mathrm{Ca}^{2+}]_{\mathrm{SR}}^{\mathrm{s,d}}\right) / \tau_{\mathrm{diff,dom,SR}} \\ & + \left([\mathrm{Ca}^{2+}]_{\mathrm{SR}}^{\mathrm{s-1,d}} + [\mathrm{Ca}^{2+}]_{\mathrm{SR}}^{\mathrm{s+1,d}} - 2 \times [\mathrm{Ca}^{2+}]_{\mathrm{SR}}^{\mathrm{s,d}}\right) / \tau_{\mathrm{diff,seg,SR}}\end{aligned}$$

$$\begin{aligned}\mathrm{J}_{\mathrm{diff,SRS}}^{\mathrm{s,d}} = {} & \left([\mathrm{Ca}^{2+}]_{\mathrm{SRS}}^{\mathrm{s,d-1}} + [\mathrm{Ca}^{2+}]_{\mathrm{SRS}}^{\mathrm{s,d+1}} - 2 \times [\mathrm{Ca}^{2+}]_{\mathrm{SRS}}^{\mathrm{s,d}}\right) / \tau_{\mathrm{diff,dom,SRS}} \\ & + \left([\mathrm{Ca}^{2+}]_{\mathrm{SRS}}^{\mathrm{s-1,d}} + [\mathrm{Ca}^{2+}]_{\mathrm{SRS}}^{\mathrm{s+1,d}} - 2 \times [\mathrm{Ca}^{2+}]_{\mathrm{SRS}}^{\mathrm{s,d}}\right) / \tau_{\mathrm{diff,seg,SRS}}\end{aligned}$$

$$\mathrm{J}_{\mathrm{diff,SRS\leftrightarrow cyt}}^{\mathrm{s,d}} = \left([\mathrm{Ca}^{2+}]_{\mathrm{SRS}}^{\mathrm{s,d}} - [\mathrm{Ca}^{2+}]_{\mathrm{cyt}}^{\mathrm{s,d}}\right) / \tau_{\mathrm{diff,SRS\leftrightarrow cyt}}$$

Similarly, Ca^{2+} diffuses between segments in both left and right subsarcolemmal compartments (*m*):

$$\tau_{\mathrm{diff,seg,subsl}} = 3.4\ \mathrm{ms}$$

$$\mathrm{J}_{\mathrm{diff,subsl}}^{\mathrm{s,m}} = \left([\mathrm{Ca}^{2+}]_{\mathrm{subsl}}^{\mathrm{s-1,m}} + [\mathrm{Ca}^{2+}]_{\mathrm{subsl}}^{\mathrm{s+1,m}} - 2 \times [\mathrm{Ca}^{2+}]_{\mathrm{subsl}}^{\mathrm{s,m}}\right) / \tau_{\mathrm{diff,seg,subsl}}$$

2.3. Changes in $[Ca^{2+}]$

For all domains (with the exception of the leftmost and rightmost) in every segment, (i.e., *d* between 1 and 16, inclusive), intracellular Ca^{2+} concentrations were updated as follows:

$$\frac{\mathrm{d}[\mathrm{Ca}^{2+}]_{\mathrm{cyt}}^{\mathrm{s,d}}}{\mathrm{dt}} = -\mathrm{J}_{\mathrm{up}}^{\mathrm{s,d}} \times \frac{\mathrm{v}_{\mathrm{SR}}}{\mathrm{v}_{\mathrm{cyt}}} - \mathrm{J}_{\mathrm{Buff,Ca,cyt}}^{\mathrm{s,d}} + \mathrm{J}_{\mathrm{diff,cyt}}^{\mathrm{s,d}} + \mathrm{J}_{\mathrm{diff,SRS\leftrightarrow cyt}}^{\mathrm{s,d}}$$

$$\frac{\mathrm{d}[\mathrm{Ca}^{2+}]_{\mathrm{SRS,tot}}^{\mathrm{s,d}}}{\mathrm{dt}} = \mathrm{J}_{\mathrm{rel}}^{\mathrm{s,d}} \times \frac{\mathrm{v}_{\mathrm{SR}}}{\mathrm{v}_{\mathrm{SRS}}} + \mathrm{J}_{\mathrm{diff,SRS}}^{\mathrm{s,d}} - \mathrm{J}_{\mathrm{diff,SRS\leftrightarrow cyt}}^{\mathrm{s,d}} \times \frac{\mathrm{v}_{\mathrm{cyt}}}{\mathrm{v}_{\mathrm{SRS}}}$$

$$\frac{\mathrm{d}[\mathrm{Ca}^{2+}]_{\mathrm{SR,tot}}^{\mathrm{s,d}}}{\mathrm{dt}} = \mathrm{J}_{\mathrm{up}}^{\mathrm{s,d}} - \mathrm{J}_{\mathrm{rel}}^{\mathrm{s,d}} + \mathrm{J}_{\mathrm{diff,SR}}^{\mathrm{s,d}}$$

For both subsarcolemmal compartments (m) in each segment:

$$\mathrm{I}_{\mathrm{Ca,subsl,tot}}^{\mathrm{s,m}} = \mathrm{I}_{\mathrm{Ca,b,subsl}}^{\mathrm{s,m}} + \mathrm{I}_{\mathrm{pCa,subsl}}^{\mathrm{s,m}} - 2 \times \mathrm{I}_{\mathrm{NCX,subsl}}^{\mathrm{s,m}}$$

$$\mathrm{k}_{\mathrm{on,SLLow}} = 100\ (\mathrm{mmol/L})^{-1}\ \mathrm{ms}^{-1}, \qquad \mathrm{k}_{\mathrm{off,SLLow}} = 1.3\ \mathrm{ms}^{-1}$$

$$\mathrm{k}_{\mathrm{on,SLHigh}} = 100\ (\mathrm{mmol/L})^{-1}\ \mathrm{ms}^{-1}, \qquad \mathrm{k}_{\mathrm{off,SLHigh}} = 0.03\ \mathrm{ms}^{-1}$$

$$[\mathrm{SLLow}]_{\mathrm{subsl,max}} = 37.4 \cdot 10^{-3} \times \frac{\mathrm{v}_{\mathrm{cyt}}}{\mathrm{v}_{\mathrm{subsl}}}$$

$$[\mathrm{SLHigh}]_{\mathrm{subsl,max}} = 13.4 \cdot 10^{-3} \times \frac{\mathrm{v}_{\mathrm{cyt}}}{\mathrm{v}_{\mathrm{subsl}}}$$

$$\frac{\mathrm{d}[\mathrm{EGTA}]_{\mathrm{bound,subsl}}^{\mathrm{s,m}}}{\mathrm{dt}} = \mathrm{k}_{\mathrm{on,EGTA}} \times [\mathrm{Ca}^{2+}]_{\mathrm{subsl}}^{\mathrm{s,m}} \times \left([\mathrm{EGTA}]_{\mathrm{max}} - [\mathrm{EGTA}]_{\mathrm{bound,subsl}}^{\mathrm{s,m}}\right)$$
$$-\mathrm{k}_{\mathrm{off,EGTA}} \times [\mathrm{EGTA}]_{\mathrm{bound,subsl}}^{\mathrm{s,m}}$$

$$\frac{\mathrm{d}[\mathrm{SLLow}]_{\mathrm{bound,subsl}}^{\mathrm{s,m}}}{\mathrm{dt}} = \mathrm{k}_{\mathrm{on,SLLow}} \times [\mathrm{Ca}^{2+}]_{\mathrm{subsl}}^{\mathrm{s,m}} \times \left([\mathrm{SLLow}]_{\mathrm{subsl,max}} - [\mathrm{SLLow}]_{\mathrm{bound,subsl}}^{\mathrm{s,m}}\right)$$
$$-\mathrm{k}_{\mathrm{off,SLLow}} \times [\mathrm{SLLow}]_{\mathrm{bound,subsl}}^{\mathrm{s,m}}$$

$$\frac{\mathrm{d}[\mathrm{SLHigh}]_{\mathrm{bound,subsl}}^{\mathrm{s,m}}}{\mathrm{dt}} = \mathrm{k}_{\mathrm{on,SLHigh}} \times [\mathrm{Ca}^{2+}]_{\mathrm{subsl}}^{\mathrm{s,m}} \times \left([\mathrm{SLHigh}]_{\mathrm{subsl,max}} - [\mathrm{SLHigh}]_{\mathrm{bound,subsl}}^{\mathrm{s,m}}\right)$$
$$-\mathrm{k}_{\mathrm{off,SLHigh}} \times [\mathrm{SLHigh}]_{\mathrm{bound,subsl}}^{\mathrm{s,m}}$$

$$\mathrm{J}_{\mathrm{Buff,Ca,subsl}}^{\mathrm{s,m}} = \frac{\mathrm{d}[\mathrm{EGTA}]_{\mathrm{bound,subsl}}^{\mathrm{s,m}}}{\mathrm{dt}} + \frac{\mathrm{d}[\mathrm{SLLow}]_{\mathrm{bound,subsl}}^{\mathrm{s,m}}}{\mathrm{dt}} + \frac{\mathrm{d}[\mathrm{SLHigh}]_{\mathrm{bound,subsl}}^{\mathrm{s,m}}}{\mathrm{dt}}$$

For the first, leftmost domain (*d*=0) connected to membrane 0:

$$\mathrm{J}_{\mathrm{diff,cyt\leftrightarrow subsl}}^{\mathrm{s,0}} = \mathrm{k}_{\mathrm{Ca,cyt\leftrightarrow subsl}} \times \left([\mathrm{Ca}^{2+}]_{\mathrm{subsl}}^{\mathrm{s,0}} - [\mathrm{Ca}^{2+}]_{\mathrm{cyt}}^{\mathrm{s,0}}\right), \qquad \mathrm{k}_{\mathrm{Ca,cyt\leftrightarrow subsl}} = 6.5486 \cdot 10^{-12}$$

$$\mathrm{J}_{\mathrm{diff,SRS\leftrightarrow subsl}}^{\mathrm{s,0}} = \mathrm{k}_{\mathrm{Ca,SRS\leftrightarrow subsl}} \times \left([\mathrm{Ca}^{2+}]_{\mathrm{subsl}}^{\mathrm{s,0}} - [\mathrm{Ca}^{2+}]_{\mathrm{SRS}}^{\mathrm{s,0}}\right), \qquad \mathrm{k}_{\mathrm{Ca,SRS\leftrightarrow subsl}} = 8.2413 \cdot 10^{-15}$$

$$\mathrm{I}_{\mathrm{Ca,SRS,tot}}^{\mathrm{s,0}} = \mathrm{I}_{\mathrm{Ca,L}}^{\mathrm{s,0}} + \mathrm{I}_{\mathrm{Ca,b,SRS}}^{\mathrm{s,0}} + \mathrm{I}_{\mathrm{pCa,SRS}}^{\mathrm{s,0}} - 2 \times \mathrm{I}_{\mathrm{NCX,SRS}}^{\mathrm{s,0}}$$

$$\frac{\mathrm{d}[\mathrm{Ca}^{2+}]_{\mathrm{cyt}}^{\mathrm{s,0}}}{\mathrm{dt}} = -\mathrm{J}_{\mathrm{up}}^{\mathrm{s,0}} \times \frac{\mathrm{v}_{\mathrm{SR}}}{\mathrm{v}_{\mathrm{cyt}}} - \mathrm{J}_{\mathrm{Buff,Ca,cyt}}^{\mathrm{s,0}} + \mathrm{J}_{\mathrm{diff,cyt\leftrightarrow subsl}}^{\mathrm{s,0}} \times \frac{0.5}{\mathrm{v}_{\mathrm{cyt}}/\mathrm{N}_{\mathrm{Dom}}} + \mathrm{J}_{\mathrm{diff,cyt}}^{\mathrm{s,0}} + \mathrm{J}_{\mathrm{diff,SRS\leftrightarrow cyt}}^{\mathrm{s,0}}$$

$$\frac{\mathrm{d}[\mathrm{Ca}^{2+}]_{\mathrm{SRS,tot}}^{\mathrm{s,0}}}{\mathrm{dt}} = \frac{-\mathrm{I}_{\mathrm{Ca,SRS,tot}}^{\mathrm{s,0}} \times \mathrm{C}_{\mathrm{mem}}}{\mathrm{v}_{\mathrm{SRS}} \times \mathrm{F} \times \mathrm{z}_{\mathrm{ca}}} + \mathrm{J}_{\mathrm{diff,SRS\leftrightarrow subsl}}^{\mathrm{s,0}} \times \frac{0.5}{\mathrm{v}_{\mathrm{SRS}}/\mathrm{N}_{\mathrm{Dom}}} + \mathrm{J}_{\mathrm{rel}}^{\mathrm{s,0}} \times \frac{\mathrm{v}_{\mathrm{SR}}}{\mathrm{v}_{\mathrm{SRS}}} + \mathrm{J}_{\mathrm{diff,SRS}}^{\mathrm{s,0}}$$
$$- \mathrm{J}_{\mathrm{diff,SRS\leftrightarrow cyt}}^{\mathrm{s,0}} \times \frac{\mathrm{v}_{\mathrm{cyt}}}{\mathrm{v}_{\mathrm{SRS}}}$$

$$\frac{\mathrm{d}[\mathrm{Ca}^{2+}]_{\mathrm{SR,tot}}^{\mathrm{s,0}}}{\mathrm{dt}} = \mathrm{J}_{\mathrm{up}}^{\mathrm{s,0}} - \mathrm{J}_{\mathrm{rel}}^{\mathrm{s,0}} + \mathrm{J}_{\mathrm{diff,SR}}^{\mathrm{s,0}}$$

$$\frac{\mathrm{d[Ca^{2+}]^{s,0}_{subsl}}}{\mathrm{dt}} = \frac{-\mathrm{I^{s,0}_{Ca,subsl,tot}}\times \mathrm{C_{mem}}}{\mathrm{v_{subsl}}\times \mathrm{F}\times \mathrm{z_{ca}}} - \frac{1}{\mathrm{v_{subsl}}}\times\left(\mathrm{J^{s,0}_{diff,SRS\leftrightarrow subsl}}+\mathrm{J^{s,0}_{diff,cyt\leftrightarrow subsl}}\right)+\mathrm{J^{s,0}_{diff,subsl}} - \mathrm{J^{s,0}_{Buff,Ca,subsl}}$$

For the last, rightmost domain (*d*=17) connected to membrane 1:

$$\mathrm{J^{s,1}_{diff,cyt\leftrightarrow subsl}} = \mathrm{k_{Ca,cyt\leftrightarrow subsl}}\times\left(\mathrm{[Ca^{2+}]^{s,1}_{subsl}} - \mathrm{[Ca^{2+}]^{s,17}_{cyt}}\right)$$

$$\mathrm{J^{s,1}_{diff,SRS\leftrightarrow subsl}} = \mathrm{k_{Ca,SRS\leftrightarrow subsl}}\times\left(\mathrm{[Ca^{2+}]^{s,1}_{subsl}} - \mathrm{[Ca^{2+}]^{s,17}_{SRS}}\right)$$

$$\mathrm{I}^{s,1}_{\mathrm{Ca,tot}} = \mathrm{I}^{s,1}_{\mathrm{Ca,L}} + \mathrm{I}^{s,1}_{\mathrm{Ca,b,SRS}} + \mathrm{I}^{s,1}_{\mathrm{pCa,SRS}} - 2\times \mathrm{I}^{s,1}_{\mathrm{NCX,SRS}}$$

$$\frac{\mathrm{d[Ca^{2+}]^{s,17}_{cyt}}}{\mathrm{dt}} = -\mathrm{J^{s,17}_{up}}\times\frac{\mathrm{v_{SR}}}{\mathrm{v_{cyt}}} - \mathrm{J^{s,17}_{Buff,Ca,cyt}} + \mathrm{J^{s,1}_{diff,cyt\leftrightarrow subsl}}\times\frac{0.5}{\mathrm{v_{cyt}/N_{Dom}}} + \mathrm{J^{s,17}_{diff,cyt}} + \mathrm{J^{s,17}_{diff,SRS\leftrightarrow cyt}}$$

$$\frac{\mathrm{d[Ca^{2+}]^{s,17}_{SRS,tot}}}{\mathrm{dt}} = \frac{\mathrm{I^{s,1}_{Ca,tot}}\times\mathrm{C_{mem}}}{\mathrm{v_{SRS}}\times\mathrm{F}\times\mathrm{z_{ca}}} + \mathrm{J^{s,1}_{diff,SRS\leftrightarrow subsl}}\times\frac{0.5}{\mathrm{v_{SRS}/N_{Dom}}} + \mathrm{J^{s,17}_{rel}}\times\frac{\mathrm{v_{SR}}}{\mathrm{v_{SRS}}} + \mathrm{J^{s,17}_{diff,SRS}} - \mathrm{J^{s,17}_{diff,SRS\leftrightarrow cyt}}\times\frac{\mathrm{v_{cyt}}}{\mathrm{v_{SRS}}}$$

$$\frac{\mathrm{d[Ca^{2+}]^{s,17}_{SR,tot}}}{\mathrm{dt}} = \mathrm{J^{s,17}_{up}} - \mathrm{J^{s,17}_{rel}} + \mathrm{J^{s,17}_{diff,SR}}$$

$$\frac{\mathrm{d[Ca^{2+}]^{s,1}_{subsl}}}{\mathrm{dt}} = \frac{-\mathrm{I^{s,1}_{Ca,subsl,tot}}\times \mathrm{C_{mem}}}{\mathrm{v_{subsl}}\times \mathrm{F}\times \mathrm{z_{ca}}} - \frac{1}{\mathrm{v_{subsl}}}\times\left(\mathrm{J^{s,1}_{diff,SRS\leftrightarrow subsl}}+\mathrm{J^{s,1}_{diff,cyt\leftrightarrow subsl}}\right)+\mathrm{J^{s,1}_{diff,subsl}} - \mathrm{J^{s,1}_{Buff,Ca,subsl}}$$

The ‘free’ concentration of $[\mathrm{Ca}^{2+}]_{\mathrm{SRS}}$ and $[\mathrm{Ca}^{2+}]_{\mathrm{SR}}$ was calculated based on the total concentrations and the known Ca^{2+}-buffer properties in each compartment, using quasi-steady-state assumptions:

$$\mathrm{Buff^{s,d}_{Ca,SRS,b}} = \mathrm{[SLLow]_{SRS,max}} + \mathrm{[SLHigh]_{SRS,max}} - \mathrm{[Ca^{2+}]^{s,d}_{SRS,tot}} + \mathrm{K_{m,SLlow}} + \mathrm{K_{m,SLhigh}}$$

$$\mathrm{Buff^{s,d}_{Ca,SRS,c}} = \mathrm{K_{m,SLlow}}\cdot\mathrm{K_{m,SLhigh}} - \mathrm{[Ca^{2+}]^{s,d}_{SRS,tot}}\cdot\left(\mathrm{K_{m,SLlow}}+\mathrm{K_{m,SLhigh}}\right) + \mathrm{[SLLow]_{SRS,max}}\cdot\mathrm{K_{m,SLhigh}} + \mathrm{[SLHigh]_{SRS,max}}\cdot\mathrm{K_{m,SLlow}}$$

$$\mathrm{Buff^{s,d}_{Ca,SRS,d}} = -\mathrm{K_{m,SLlow}}\cdot\mathrm{K_{m,SLhigh}}\cdot\mathrm{[Ca^{2+}]^{s,d}_{SRS,tot}}$$

$$\mathrm{K_{m,SLlow}} = \frac{\mathrm{k_{off,SLLow}}}{\mathrm{k_{on,SLLow}}},\qquad \mathrm{K_{m,SLhigh}} = \frac{\mathrm{k_{off,SLHigh}}}{\mathrm{k_{on,SLHigh}}}$$

$$\mathrm{[SLLow]_{SRS,max}} = 4.6\cdot 10^{-4}\times\frac{\mathrm{v_{cyt}}}{\mathrm{v_{SRS}}},\qquad \mathrm{[SLHigh]_{SRS,max}} = 1.65\cdot 10^{-4}\times\frac{\mathrm{v_{cyt}}}{\mathrm{v_{SRS}}}$$

$$\mathrm{[Ca^{2+}]^{s,d}_{SRS}} = -\frac{1}{3}\times\mathrm{Buff^{s,d}_{Ca,SRS,b}} + \frac{2}{3}\times\sqrt{\left(\mathrm{Buff^{s,d}_{Ca,SRS,b}}\right)^2 - 3\times\mathrm{Buff^{s,d}_{Ca,SRS,c}}} \times\cos\left(\frac{1}{3}\cos^{-1}\left(\frac{9\times\mathrm{Buff^{s,d}_{Ca,SRS,b}}\times\mathrm{Buff^{s,d}_{Ca,SRS,c}} - 2\times\left(\mathrm{Buff^{s,d}_{Ca,SRS,b}}\right)^3 - 27\times\mathrm{Buff^{s,d}_{Ca,SRS,d}}}{2\times\left(\left(\mathrm{Buff^{s,d}_{Ca,SRS,b}}\right)^2 - 3\times\mathrm{Buff^{s,d}_{Ca,SRS,c}}\right)^{1.5}}\right)\right)$$

$$[\mathrm{CSQN}]_{\mathrm{max}} = 0.14 \times \frac{\mathrm{v}_{\mathrm{cyt}}}{\mathrm{v}_{\mathrm{SR}}}, \qquad \mathrm{K}_{\mathrm{m,CSQN}} = 0.65\ \mathrm{mmol/L}$$

$$\mathrm{Buff}^{\mathrm{s,d}}_{\mathrm{Ca,SR,b}} = [\mathrm{Ca}^{2+}]^{\mathrm{s,d}}_{\mathrm{SR,tot}} + [\mathrm{CSQN}]_{\mathrm{max}} + \mathrm{K}_{\mathrm{m,CSQN}}$$

$$\mathrm{Buff}^{\mathrm{s,d}}_{\mathrm{Ca,SR,c}} = [\mathrm{Ca}^{2+}]^{\mathrm{s,d}}_{\mathrm{SR,tot}} \times [\mathrm{CSQN}]_{\mathrm{max}}$$

$$[\mathrm{CSQN}]_{\mathrm{bound}} = \frac{1}{2} \times \left(\mathrm{Buff}^{\mathrm{s,d}}_{\mathrm{Ca,SR,b}} - \sqrt{\left(\mathrm{Buff}^{\mathrm{s,d}}_{\mathrm{Ca,SR,b}}\right)^2 - 4 \times \mathrm{Buff}^{\mathrm{s,d}}_{\mathrm{Ca,SR,c}}} \right)$$

$$[\mathrm{Ca}^{2+}]^{\mathrm{s,d}}_{\mathrm{SR}} = [\mathrm{Ca}^{2+}]^{\mathrm{s,d}}_{\mathrm{SR,tot}} - [\mathrm{CSQN}]_{\mathrm{bound}}$$

3. Ryanodine Receptor Channel

We employed the 4-state Markov model of the human atrial action potential (AP) model by Grandi et al.[11] to simulate RyR2 gating (**Online Figure IVA**). The model structure reflects activation (left and right halves of the Markov model), predominantly by an increase in [Ca^{2+}] in the SRS, and regulation by SR Ca^{2+} (top and bottom halves of the Markov model). The mechanisms controlling termination of Ca^{2+}-induced Ca^{2+}-release and subsequent refractoriness of RyR2 remain an area of intensive investigation.[13] Recent research has suggested several potential contributing mechanisms. Although direct inactivation of RyR2 appears unlikely, there is strong evidence for regulation of RyR2 activity by luminal [Ca^{2+}].[14] The lower half of the model reflects such a non-conducting 'inactivated' state which is controlled by luminal Ca^{2+}. Model parameters were optimized such that the model operates around a steady-state SR Ca^{2+}-load that is consistent with experimental observations and is able to reproduce key properties of single-channel RyR2 recordings obtained in bilayer experiments with RyR2 from human atrial samples (**Online Figure IVB,C**).[15] For the pAF model, RyR2 open probability at diastolic [Ca^{2+}] (150 nmol/L) was increased 4 fold, in line with experimental findings (**Online Figure V**; **Online Table III**). Stochastic gating of single RyR2 was simulated as recently described for a stochastic model of the canine ventricular myocyte.[16] Briefly, for every state in the Markov model the number of channels making a transition to every other state within the time period Δt (in ms) is determined using a random number from a Binomial distribution based on the number of channels in this state and the individual transition rates ($k_{x\text{-}y}$ in ms^{-1}) to neighboring states.[16]

For the RyR2 in segment *s* and domain *d*, the transition rates and release flux are determined as follows:

$$\mathrm{P}[0]_{\mathrm{RyR2}} = \begin{cases} 0.2, & (\mathrm{Ctl}) \\ 0.4, & (\mathrm{pAF}) \end{cases}, \qquad \mathrm{P}[1]_{\mathrm{RyR2}} = \begin{cases} 0.22, & (\mathrm{Ctl}) \\ 0.24, & (\mathrm{pAF}) \end{cases}, \qquad \mathrm{P}[2]_{\mathrm{RyR2}} = 12$$

$$\mathrm{P}[3]_{\mathrm{RyR2}} = 1.0, \qquad \mathrm{P}[4]_{\mathrm{RyR2}} = 20$$

$$\mathrm{P}[5]_{\mathrm{RyR2}} = \begin{cases} 0.0035, & (\mathrm{Ctl}) \\ 0.0105, & (\mathrm{pAF}) \end{cases}, \qquad \mathrm{P}[6]_{\mathrm{RyR2}} = 0.63$$

$$\mathrm{P}[7]_{\mathrm{RyR2}} = 9.0 \cdot 10^{-4}, \qquad \mathrm{P}[8]_{\mathrm{RyR2}} = 0.8 \cdot 10^{-4}, \qquad \mathrm{P}[9]_{\mathrm{RyR2}} = 1.75$$

$$\mathrm{P}[10]_{\mathrm{RyR2}} = 6.3, \qquad \mathrm{P}[11]_{\mathrm{RyR2}} = 0.007\ (0.014\ \text{in the presence of caffeine})$$

$$\mathrm{Inact}_{\infty}^{s,d}=\frac{\mathrm{P[0]_{RyR2}}}{1+\left(\frac{[\mathrm{Ca^{2+}}]_{\mathrm{SR}}^{s,d}}{4}\right)^{4}}+\frac{1-\mathrm{P[0]_{RyR2}}}{1+\left(\frac{[\mathrm{Ca^{2+}}]_{\mathrm{SR}}^{s,d}}{\mathrm{P[1]_{RyR2}}}\right)^{\mathrm{P[2]_{RyR2}}}}$$

$$\tau_{\mathrm{Inact}}^{s,d}=\mathrm{P[3]_{RyR2}}+\frac{\mathrm{P[4]_{RyR2}}}{1+\left(\frac{\mathrm{P[1]}}{[\mathrm{Ca^{2+}}]_{\mathrm{SR}}^{s,d}}\right)^{\mathrm{P[2]}}}$$

$$\frac{d\mathrm{IR}^{s,d}}{dt}=\mathrm{J}_{\mathrm{rel}}^{s,d}-\frac{0.1}{1+\exp\left(\left(\mathrm{J}_{\mathrm{rel}}^{s,d}-1.5\cdot10^{-3}\right)/1.0\cdot10^{-4}\right)}\times\mathrm{IR}^{s,d}$$

$$\mathrm{Co}_{\mathrm{RyR}}^{s,d}=\frac{1}{1+\left(\frac{\mathrm{IR}^{s,d}}{0.5}\right)^{8}}$$

$$\mathrm{Act}_{\infty}^{s,d}=\mathrm{Co}_{\mathrm{RyR}}^{s,d}\times\left(\mathrm{P[5]_{RyR2}}+\frac{\mathrm{P[6]_{RyR2}}}{1+\exp\left(\left([\mathrm{Ca^{2+}}]_{\mathrm{SRS}}^{s,d}-\mathrm{P[7]_{RyR2}}\right)/\mathrm{P[8]_{RyR2}}\right)}\right)$$

$$\mathrm{Act}_{\infty,\mathrm{low}}^{s,d}=\mathrm{Co}_{\mathrm{RyR}}^{s,d}\times\left(\mathrm{P[5]_{RyR2}}+\frac{\mathrm{P[6]_{RyR2}}}{1+\exp\left(\left([\mathrm{Ca^{2+}}]_{\mathrm{SRS}}^{s,d}-\mathrm{P[7]_{RyR2}}\times\mathrm{P[9]_{RyR2}}\right)/\mathrm{P[8]_{RyR2}}\right)}\right)$$

$$\tau_{\mathrm{Act}}^{s,d}=\mathrm{P[10]_{RyR2}}$$

$$k_{\mathrm{C-O}}^{s,d}=\frac{\mathrm{Act}_{\infty}^{s,d}}{\tau_{\mathrm{Act}}^{s,d}},\qquad k_{\mathrm{O-C}}^{s,d}=\frac{1-\mathrm{Act}_{\infty}^{s,d}}{\tau_{\mathrm{Act}}^{s,d}}$$

$$k_{\mathrm{CI-OI}}^{s,d}=\frac{\mathrm{Act}_{\infty,\mathrm{low}}^{s,d}}{\tau_{\mathrm{Act}}^{s,d}},\qquad k_{\mathrm{OI-CI}}^{s,d}=\frac{1-\mathrm{Act}_{\infty,\mathrm{low}}^{s,d}}{\tau_{\mathrm{Act}}^{s,d}}$$

$$k_{\mathrm{O-OI}}^{s,d}=\frac{\mathrm{Inact}_{\infty}^{s,d}}{\tau_{\mathrm{Inact}}^{s,d}},\qquad k_{\mathrm{OI-O}}^{s,d}=\frac{1-\mathrm{Inact}_{\infty}^{s,d}}{\tau_{\mathrm{Inact}}^{s,d}}$$

$$k_{\mathrm{CI-C}}^{s,d}=0.1\times k_{\mathrm{OI-O}},\qquad k_{\mathrm{C-CI}}^{s,d}=\frac{k_{\mathrm{C-O}}\times k_{\mathrm{O-OI}}\times k_{\mathrm{OI-CI}}\times k_{\mathrm{CI-C}}}{k_{\mathrm{CI-OI}}\times k_{\mathrm{OI-O}}\times k_{\mathrm{O-C}}}$$

$$\mathrm{J}_{\mathrm{rel}}^{s,d}=\mathrm{P[11]_{RyR2}}\times\mathrm{N_{domains}}\times n_{\mathrm{O}}^{s,d}/\left(\frac{\mathrm{N_{RyR}}}{\mathrm{N_{domains}}\times\mathrm{N_{segments}}}\right)\times\left([\mathrm{Ca^{2+}}]_{\mathrm{SR}}^{s,d}-[\mathrm{Ca^{2+}}]_{\mathrm{SRS}}^{s,d}\right)$$

4. L-type Ca^{2+}-channel

We updated the L-type Ca^{2+}-current ($I_{Ca,L}$) formulation of the model to the Markov model developed by Decker et al.[17] (**Online Figure VIA**) in order to simulate an appropriate balance between voltage- and Ca^{2+}-dependent inactivation. This model incorporates channel activation (left-to-right transitions) and inactivation (front-to-back transitions) in the absence (lower tier) or presence of Ca^{2+} (upper tier). The model is able to reproduce voltage dependence of $I_{Ca,L}$ activation (**Online Figure VIB**) and steady-state inactivation (**Online Figure VIC**) recorded in human atrial myocytes in the presence of EGTA.[18, 19] We have previously performed simultaneous measurements of $I_{Ca,L}$ and Ca^{2+}-transients in response to a depolarization to +10 mV in atrial myocytes isolated from patients in sinus rhythm in the absence of EGTA. The model was able to reproduce the amplitude and integral of $I_{Ca,L}$ under these conditions (**Online Figure VID**).

L-type Ca^{2+}-channels were located in both left and right membrane domains *m* of each segment *s*. All L-type Ca^{2+}-channels were assumed to sense and modulate the $[Ca^{2+}]$ in the nearest junctional SR Ca^{2+}-release space, providing a microdomain for the initiation of Ca^{2+}-induced Ca^{2+}-release and the subsequent propagation of the Ca^{2+} wave towards the cell center.

$$[\mathrm{Ca}^{2+}]_{\mathrm{obs}}^{s,m} = \begin{cases} [\mathrm{Ca}^{2+}]_{\mathrm{SRS}}^{s,0}, \text{if m} = \text{left membrane} \\ [\mathrm{Ca}^{2+}]_{\mathrm{SRS}}^{s,N_{\mathrm{Dom}}-1}, \text{if m} = \text{right membrane} \end{cases}$$

$$\mathrm{ACT}_{\tau} = 0.59 + 0.8 \cdot \frac{\exp\left(0.052 \cdot (V_m + 13)\right)}{1 + \exp\left(0.132 \cdot (V_m + 13)\right)}$$

$$\mathrm{ACT}_{\infty} = \frac{1}{\left(1 + \exp\left(-\frac{V_m - 13.56}{9.45}\right)\right) \cdot \left(1 + \exp\left(-\frac{V_m + 25}{5}\right)\right)}$$

$$\alpha_{\mathrm{Ca,L}} = \frac{\mathrm{ACT}_{\infty}}{\mathrm{ACT}_{\tau}}, \qquad \beta_{\mathrm{Ca,L}} = \frac{1 - \mathrm{ACT}_{\infty}}{\mathrm{ACT}_{\tau}}$$

$$\mathrm{I}_{V,\infty} = \frac{1}{1.2474} \cdot \left(0.2474 + \frac{1}{1 + \exp\left((V_m + 17.5)/3\right)}\right)$$

$$\mathrm{Is}_{V,\infty} = \frac{1}{1.001} \cdot \left(0.001 + \frac{1}{1 + \exp\left((V_m + 17.5)/3\right)}\right)$$

$$\mathrm{I}_{V,\tau} = \frac{1}{\frac{1}{70.0 \cdot \left(1 + \exp\left((V_m + 49.10)/10.349\right)\right)} + \frac{1}{26.553 \cdot \left(1 + \exp(-(V_m + 0.213)/10.807)\right)}}$$

$$\mathrm{Is}_{\mathrm{Ca}}^{s,m} = 13.825 - \frac{6.3836}{1 + \left(\frac{3.500 \cdot 10^{-4}}{[\mathrm{Ca}^{2+}]_{\mathrm{obs}}^{s,m}}\right)^4}$$

$$\mathrm{Is}_{V,\tau}^{s,m} = \frac{1}{\frac{1}{70.0 \cdot \left(1 + \exp\left((V_m + 49.10)/10.349\right)\right)} + \frac{1}{\mathrm{Is}_{\mathrm{Ca}}^{s,m} = \left(1 + \exp(-(V_m + 0.213)/10.807)\right)}}$$

$$x_{\mathrm{Ca,L}} = \frac{\mathrm{I}_{V,\infty}}{\mathrm{I}_{V,\tau}}, \qquad y_{\mathrm{Ca,L}} = \frac{1 - \mathrm{I}_{V,\infty}}{\mathrm{I}_{V,\tau}}$$

$$xs_{\mathrm{Ca,L}}^{s,m} = \frac{\mathrm{Is}_{V,\infty}}{\mathrm{Is}_{V,\tau}}, \qquad ys_{\mathrm{Ca,L}}^{s,m} = \frac{1 - \mathrm{Is}_{V,\infty}}{\mathrm{Is}_{V,\tau}}$$

$$\delta_{\mathrm{Ca,L}}^{s,m} = \frac{14.9186}{1 + \left(\frac{1.100 \cdot 10^{-3}}{[\mathrm{Ca}^{2+}]_{\mathrm{obs}}^{s,m}}\right)^4}, \qquad \theta_{\mathrm{Ca,L}} = 1$$

$$\theta I_{Ca,L} = 1.0 \cdot 10^{-6}, \qquad \delta I_{Ca,L}^{s,m} = \theta I_{Ca,L} \cdot \frac{x_{Ca,L} \cdot ys_{Ca,L}^{s,m} \cdot \delta_{Ca,L}^{s,m}}{y_{Ca,L} \cdot xs_{Ca,L}^{s,m} \cdot \theta_{Ca,L}}$$

$$\frac{dC_{Ca,L}^{s,m}}{dt} = -\left(\alpha_{Ca,L} + \delta_{Ca,L}^{s,m} + y_{Ca,L}\right) \cdot C_{Ca,L}^{s,m} + \beta_{Ca,L} \cdot O_{Ca,L}^{s,m} + \theta_{Ca,L} \cdot Cs_{Ca,L}^{s,m} + x_{Ca,L} \cdot CI_{Ca,L}^{s,m}$$

$$\frac{dO_{Ca,L}^{s,m}}{dt} = -\left(\beta_{Ca,L} + \delta_{Ca,L}^{s,m} + y_{Ca,L}\right) \cdot O_{Ca,L}^{s,m} + \alpha_{Ca,L} \cdot C_{Ca,L}^{s,m} + \theta_{Ca,L} \cdot Os_{Ca,L}^{s,m} + x_{Ca,L} \cdot OI_{Ca,L}^{s,m}$$

$$\frac{dCs_{Ca,L}^{s,m}}{dt} = -\left(\alpha_{Ca,L} + \theta_{Ca,L} + ys_{Ca,L}^{s,m}\right) \cdot Cs_{Ca,L}^{s,m} + \delta_{Ca,L}^{s,m} \cdot C_{Ca,L}^{s,m} + \beta_{Ca,L} \cdot Os_{Ca,L}^{s,m} + xs_{Ca,L}^{s,m} \cdot CIs_{Ca,L}^{s,m}$$

$$\frac{dOs_{Ca,L}^{s,m}}{dt} = -\left(\beta_{Ca,L} + \theta_{Ca,L} + ys_{Ca,L}^{s,m}\right) \cdot Os_{Ca,L}^{s,m} + \delta_{Ca,L}^{s,m} \cdot O_{Ca,L}^{s,m} + \alpha_{Ca,L} \cdot Cs_{Ca,L}^{s,m} + xs_{Ca,L}^{s,m} \cdot OIs_{Ca,L}^{s,m}$$

$$\frac{dCI_{Ca,L}^{s,m}}{dt} = -\left(\alpha_{Ca,L} + \delta I_{Ca,L}^{s,m} + x_{Ca,L}\right) \cdot CI_{Ca,L}^{s,m} + y_{Ca,L} \cdot C_{Ca,L}^{s,m} + \theta I_{Ca,L} \cdot CIs_{Ca,L}^{s,m} + \beta_{Ca,L} \cdot OI_{Ca,L}^{s,m}$$

$$\frac{dOI_{Ca,L}^{s,m}}{dt} = -\left(\beta_{Ca,L} + \delta I_{Ca,L}^{s,m} + x_{Ca,L}\right) \cdot OI_{Ca,L}^{s,m} + y_{Ca,L} \cdot O_{Ca,L}^{s,m} + \theta I_{Ca,L} \cdot OIs_{Ca,L}^{s,m} + \alpha_{Ca,L} \cdot CI_{Ca,L}^{s,m}$$

$$\frac{dCIs_{Ca,L}^{s,m}}{dt} = -\left(\alpha_{Ca,L} + \theta I_{Ca,L} + xs_{Ca,L}^{s,m}\right) \cdot CIs_{Ca,L}^{s,m} + \delta I_{Ca,L}^{s,m} \cdot CI_{Ca,L}^{s,m} + ys_{Ca,L}^{s,m} \cdot Cs_{Ca,L}^{s,m} + \beta_{Ca,L} \cdot OIs_{Ca,L}^{s,m}$$

$$\frac{dOIs_{Ca,L}^{s,m}}{dt} = -\left(\beta_{Ca,L} + \theta I_{Ca,L} + xs_{Ca,L}^{s,m}\right) \cdot OIs_{Ca,L}^{s,m} + \delta I_{Ca,L}^{s,m} \cdot OI_{Ca,L}^{s,m} + ys_{Ca,L}^{s,m} \cdot Os_{Ca,L}^{s,m} + \alpha_{Ca,L} \cdot CIs_{Ca,L}^{s,m}$$

$$P_{Ca,L} = 1.7 \cdot 10^{-4}\ \frac{cm}{s}, \qquad \gamma_{Ca,i} = 1.0, \qquad \gamma_{Ca,o} = 0.341$$

$$\bar{I}_{Ca,L}^{s,m} = P_{Ca,L} \cdot (z_{Ca})^2 \cdot \frac{V_m \cdot F^2}{R \cdot T} \cdot \frac{\gamma_{Ca,i} \cdot [Ca^{2+}]_{obs}^{s,m} \cdot \exp\left(z_{Ca} \cdot V_m \cdot \frac{F}{R \cdot T}\right) - \gamma_{Ca,o} \cdot [Ca^{2+}]_o}{\exp\left(z_{Ca} \cdot V_m \cdot \frac{F}{R \cdot T}\right) - 1}$$

$$I_{Ca,L}^{s,m} = \bar{I}_{Ca,L}^{s,m} \cdot \left(O_{Ca,L}^{s,m} + Os_{Ca,L}^{s,m}\right)$$

5. SR Ca^{2+}-Uptake

We updated SR Ca^{2+}-uptake formulation from the Grandi et al.[11] model to reproduce experimentally observed Ca^{2+}-handling properties in every segment s and domain d:

$$J_{up}^{s,d} = J_{up,max} \times \left(\left(\frac{[Ca^{2+}]_{cyt}^{s,d}}{K_{m,up,f}}\right)^{1.787} - \left(\frac{[Ca^{2+}]_{SR}^{s,d}}{K_{m,up,r}}\right)^{1.787}\right)$$

$$K_{m,up,f} = \begin{cases} 6.25 \cdot 10^{-4} \mathrm{mmol/L\ (SR)} \\ 3.125 \cdot 10^{-4} \mathrm{mmol/L\ (pAF)} \end{cases}, \qquad K_{m,up,r} = \begin{cases} 1.0\ \mathrm{mmol/L\ (SR)} \\ 1.5\ \mathrm{mmol/L\ (pAF)} \end{cases}$$

6. Miscellaneous

The maximum conductance of the background Ca^{2+}-current ($I_{Ca,b}$) was increased by 85% compared to the Grandi et al.[11] based on experimentally observed diastolic $[Ca^{2+}]_i$ levels. Similarly, the maximum rate of Ca^{2+}extrusion via the Na^+-Ca^{2+}-

exchange current (I_{NCX}) was increased by 35% based on the rate of caffeine-induced Ca^{2+}-transient decay. Simulations were performed using fixed intracellular $[Na^+]$ of 8.5 mmol/L

7. Simulation of pAF

We developed a computational model of the human pAF myocyte by incorporating the molecular and functional experimental data obtained in pAF myocytes into the control model (**Online Table IV**, all other parameters remained unaltered). The pAF model was subsequently validated using whole-cell Ca^{2+}-handling properties of pAF myocytes (**Online Figure VII**).

Online Table IV: Model alterations to simulate pAF

Element	Parameter	Change from Ctl	Underlying Evidence
Serca2a	$K_{m,up,f}$	-50%	Increased Ser16-PLB phosphorylation (**Figure 5A**), used to match SR Ca^{2+} load
	$K_{m,up,r}$	+50%	Increased Ser16-PLB phosphorylation (**Figure 5A**), used to match increased Ca^{2+}-transient decay
	$J_{up,max}$	-25%	Reduced Serca2a protein expression (**Figure 5A**)
RyR2	N_{RyR} $P[11]_{RyR}$	+64%	Increased RyR2 protein expression in SR fractions (**Figure 6E**)
	$P[0]_{RyR}$	+100%	Altered RyR2 property to balance open probability (**Online Figure III**) and SR Ca^{2+} leak (**Online Figure V**)
	$P[1]_{RyR}$	+9%	Altered RyR2 property to balance open probability (**Online Figure III**) and Ca^{2+}-transient amplitude (**Online Figure V**)
	$P[5]_{RyR}$	+200%	Increased RyR2 single-channel open probability (**Figure 6F**, **Online Figure III**)
Other	$\tau_{diff,dom,cyt}$	+200%	Slowed $[Ca^{2+}]_i$ diffusion to slightly slow the decay of caffeine-induced Ca^{2+}-transient (**Figure 4C**)

8. Simulation of Flecainide Effects on RyR2

The effects of flecainide on RyR2 were simulated by extending the RyR2 Markov model with a blocked tier, representing channels with a flecainide molecule bound. Channels can transition between the two tiers through the open state, in line with the open-state block of RyR2 by flecainide identified by Hilliard et al.[20] (**Online Figure IXA**). The model was parameterized using RyR2 single-channel recordings in lipid bilayers.[21] In both experiments and model, RyR2 were activated using high cytosolic [Ca^{2+}] (100 μmol/L) and the relative reduction in RyR2 open probability at various concentrations of flecainide was reproduced (**Online Figure IXB,C**). Importantly, reduced RyR2 open probability was due to a reduction in open time (and not due to prolongation of closed times as is for example the case with tetracaine; **Online Figure IXC**), thereby reproducing a key characteristic of flecainide-induced RyR2 inhibition.[21]

Transition rates between states were the same in the blocked and non-blocked tiers. Transition rates between the two tier depended on flecainide concentration, as follows:

$$\mathrm{FlecB}_{\infty}^{\mathrm{s,d}} = \frac{1}{1+\left(\frac{50}{[\mathrm{Flecainide}]}\right)^{1.5}}$$

$$\tau_{\mathrm{FlecB}}^{\mathrm{s,d}} = 0.5\ \mathrm{ms}$$

$$\mathrm{k}_{\mathrm{O-OB}}^{\mathrm{s,d}} = \frac{\mathrm{FlecB}_{\infty}^{\mathrm{s,d}}}{\tau_{\mathrm{FlecB}}^{\mathrm{s,d}}}, \qquad \mathrm{k}_{\mathrm{OB-O}}^{\mathrm{s,d}} = \frac{1-\mathrm{FlecB}_{\infty}^{\mathrm{s,d}}}{\tau_{\mathrm{FlecB}}^{\mathrm{s,d}}}$$

The effects of different concentrations of flecainide on spontaneous SR Ca^{2+}-release events (SCaEs) were subsequently evaluated in the Ctl and pAF models (**Online Figure X**).

Online Figures

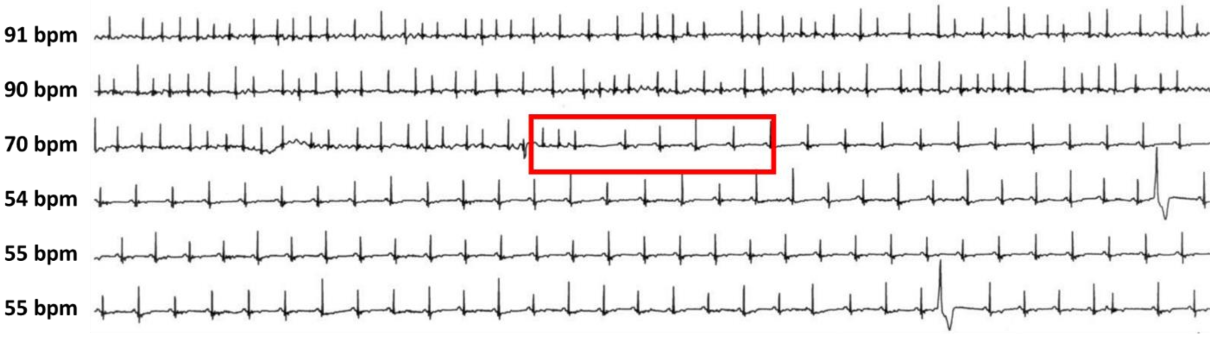

Online Figure I. ECG-holter recording of spontaneous AF conversion to sinus rhythm (red box) in a patient with paroxysmal AF. The total duration of the AF episode was about 5 hours. Each line represents 30 s of a continuous ECG-holter recording.

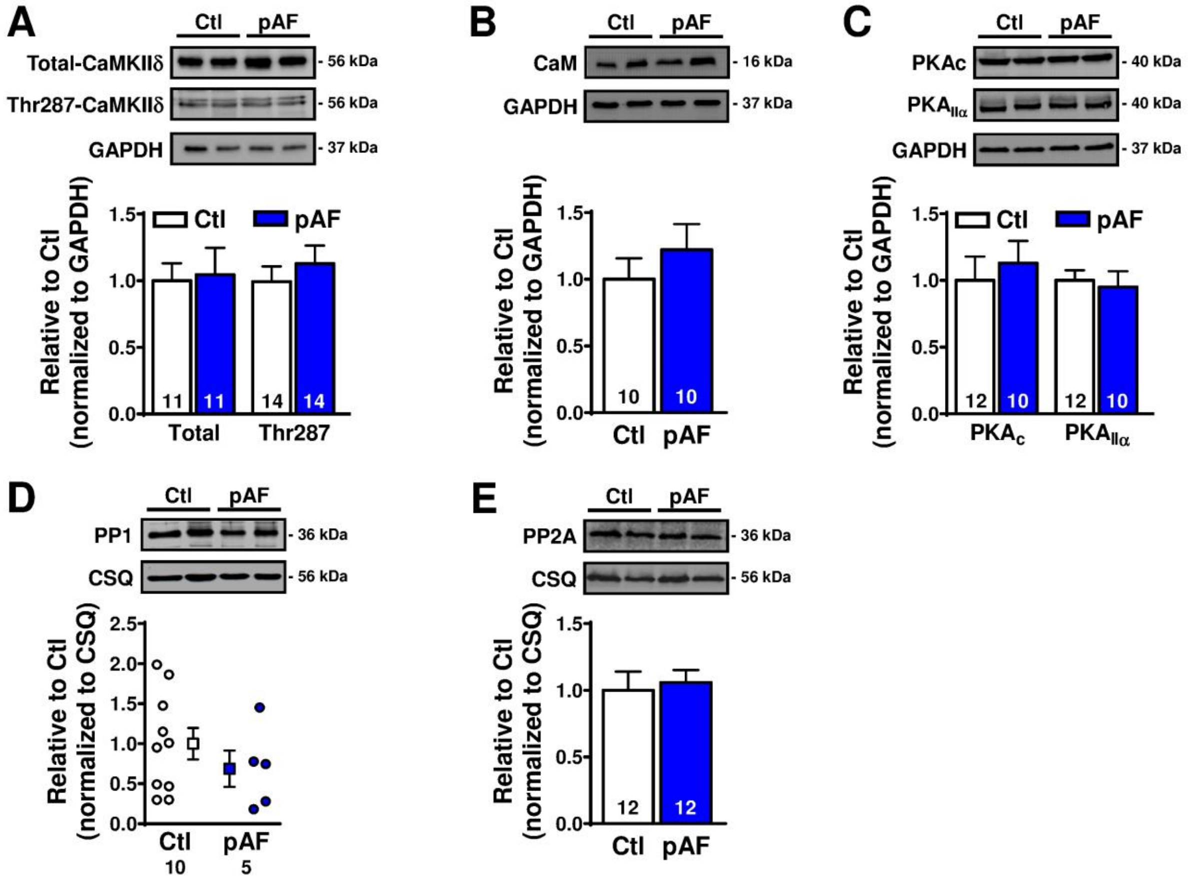

Online Figure II. Representative Western blots and quantification of protein levels in right-atrial samples of patients with sinus rhythm (Ctl) or paroxysmal AF (pAF). **A.** Total and Thr287-phosphorylated Ca^{2+}/calmodulin-dependent protein kinase-II (CaMKII). **B.** Calmodulin (CaM). **C.** Protein kinase-A (PKA) catalytic and regulatory IIα-subunit. **D.** Protein phosphatase type-1 (PP1) catalytic subunit. **E.** Protein phosphatase type-2A (PP2A) catalytic subunit. Data were normalized to calsequestrin (CSQ) or GAPDH and are shown relative to Ctl. Dot-plots were used for experiments with fewer than 10 samples. Numbers within columns or above symbols indicate number of samples. Comparisons using one-way ANOVA.

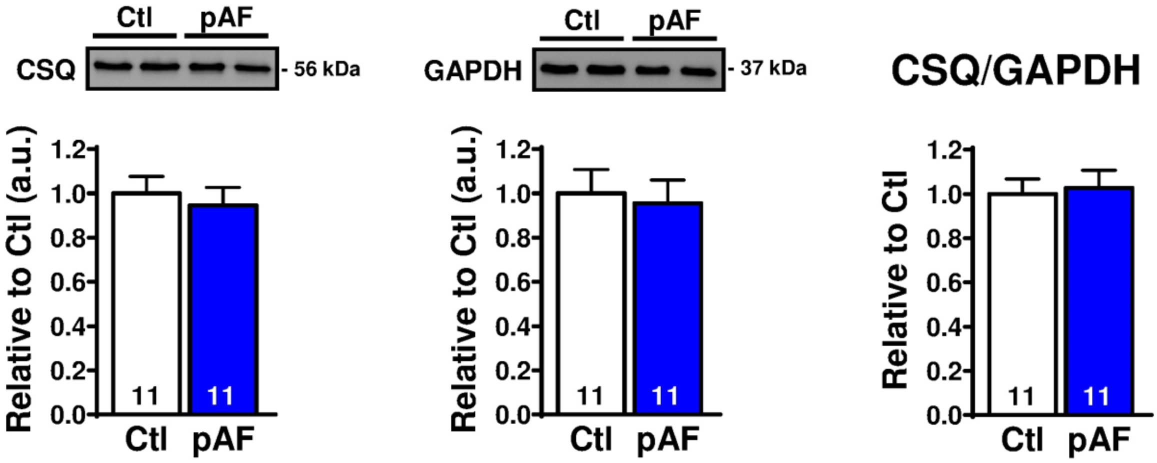

Online Figure III. Representative Western blots and quantification of protein levels of calsequestrin (CSQ; left panel) and GAPDH (middle panel) in right-atrial samples of patients with sinus rhythm (Ctl) or paroxysmal AF (pAF). Right panel shows quantification of CSQ normalized to GAPDH. Data are shown relative to Ctl expression levels. Numbers within columns indicate number of tissue samples. Comparisons using one-way ANOVA.

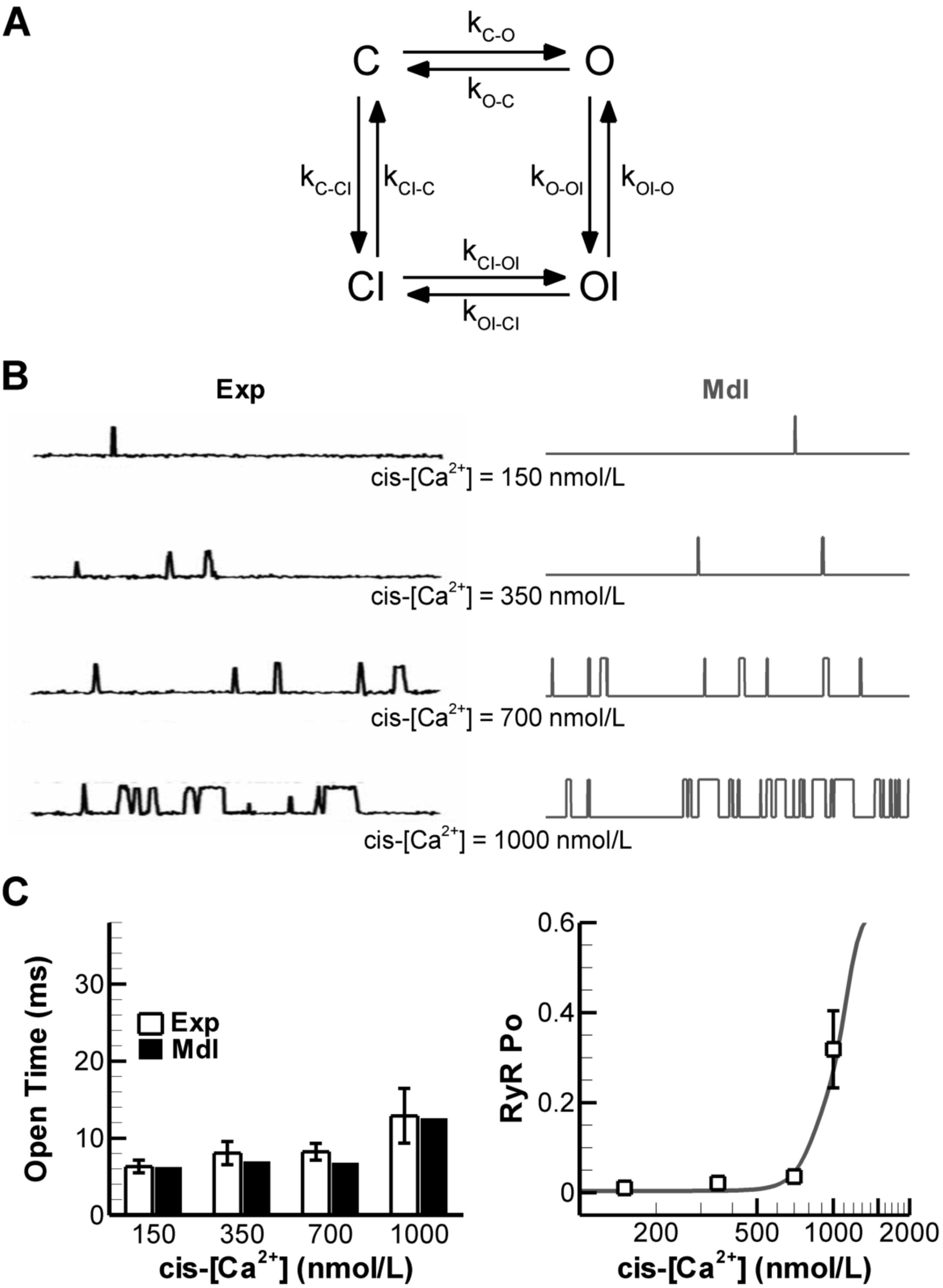

Online Figure IV. Validation of RyR2 single-channel properties. **A.** RyR2 Markov model structure. **B.** Single-channel recordings of RyR2 isolated from human atrial myocytes of patients in sinus rhythm (left panel, experimental data from Voigt et al.[15]) or stochastic simulation of single RyR2 (right panel) at different concentrations of (cytosolic) *cis*-[Ca^{2+}]. **C.** Average open time of single RyR2 (left panel) and open probability (right panel) at increasing concentrations of *cis*-[Ca^{2+}] in experiments[15] (white bars / symbols) and stochastic RyR2 model (black bars / line).

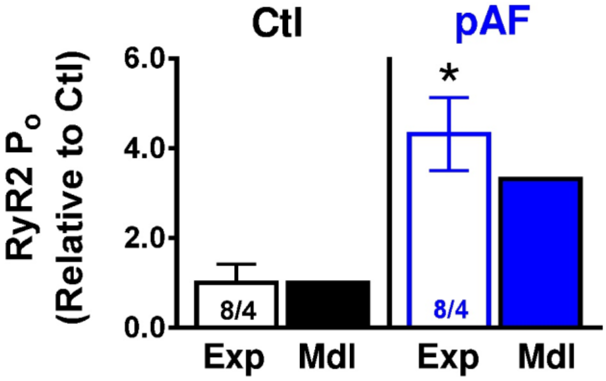

Online Figure V. Validation of relative increase in RyR2 open probability (P_o) in pAF compared to Ctl in model and experiment at diastolic cytosolic *cis*-$[Ca^{2+}]_i$ (150 nmol/L)

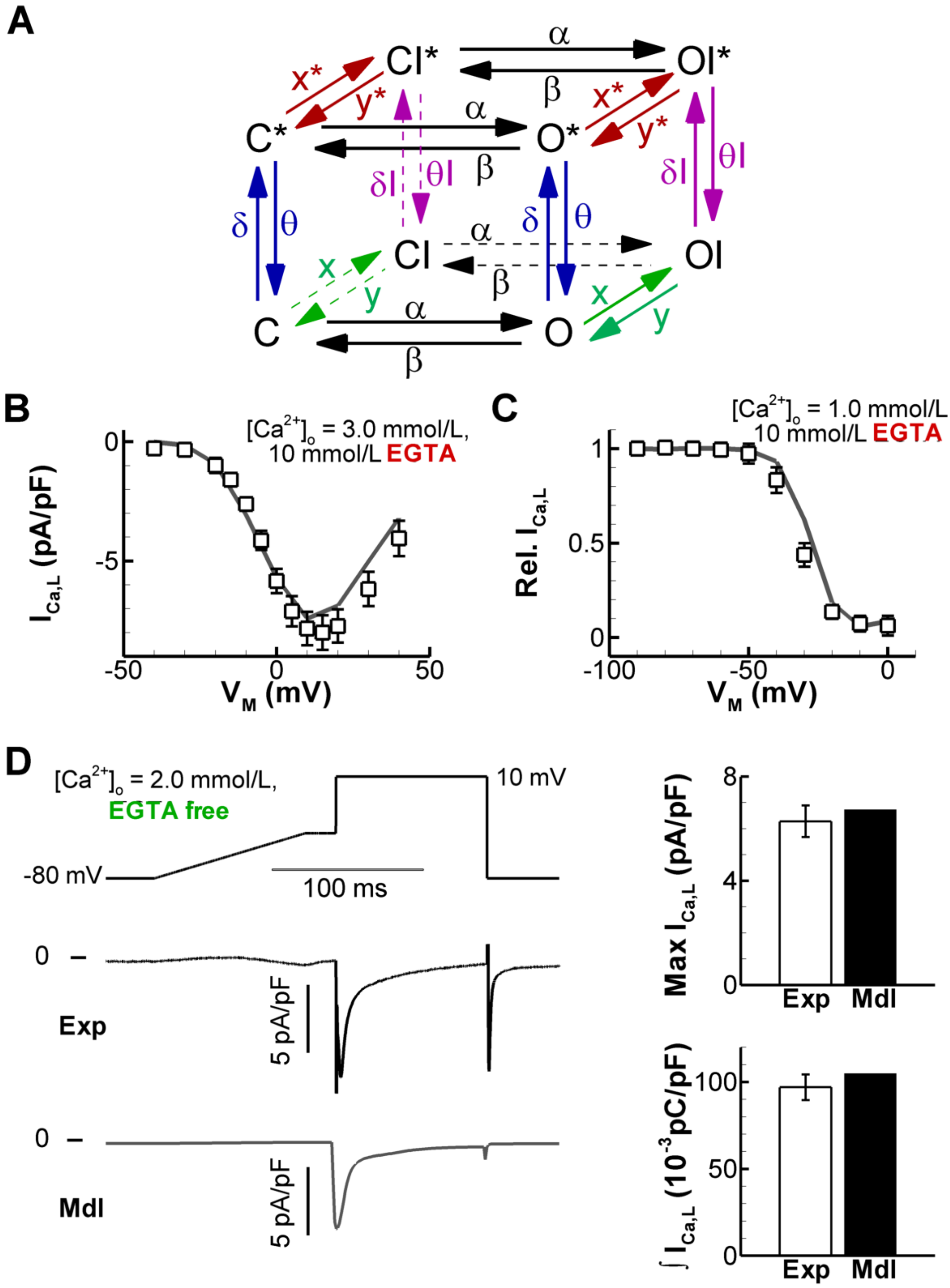

Online Figure VI. Validation of $I_{Ca,L}$ properties. **A.** Markov model structure of the $I_{Ca,L}$ model, based on Decker et al.[17] **B.** Validation of peak $I_{Ca,L}$ I-V relationship in the presence of 10 mmol/L EGTA and 3.0 mmol/L extracellular $[Ca^{2+}]$. Experimental data from Christ et al.[19] **C.** Validation of $I_{Ca,L}$ inactivation in the presence of EGTA. Experimental data from Van Wagoner et al.[18] **D.** Validation of peak and integrated $I_{Ca,L}$ in the Ctl model compared to experimental recordings in Ctl patients obtained in the absence of EGTA.

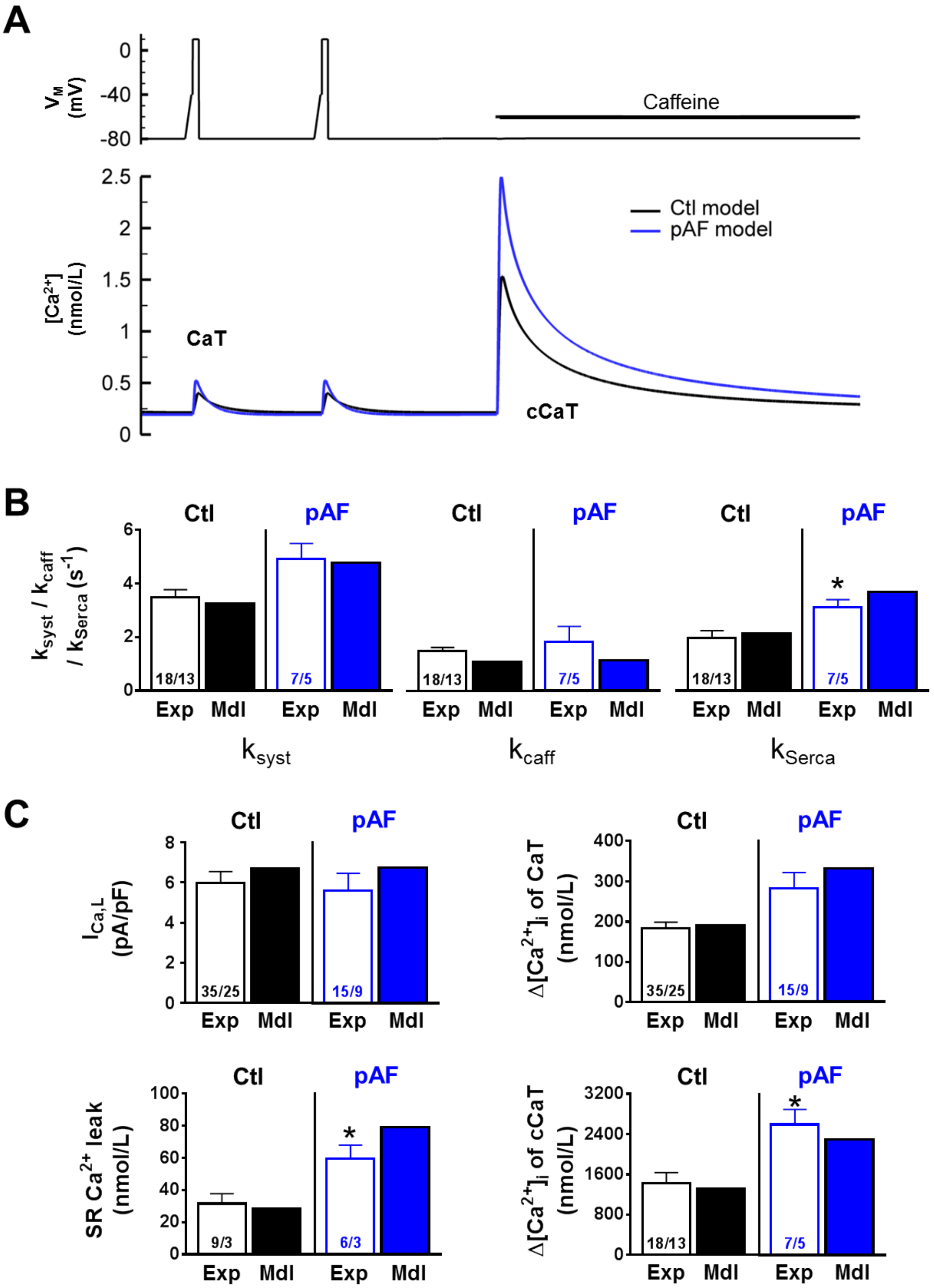

Online Figure VII. Validation of paroxysmal AF (pAF) model properties. **A.** Depolarization-induced and caffeine-induced Ca^{2+}-transient (CaT and cCaT, respectively) in Ctl (black line) and pAF (blue line) models. **B.** Validation of the rate of decay of the systolic CaT (reflecting SR Ca^{2+}-uptake by Serca2a and Ca^{2+}-extrusion by NCX), cCaT (reflecting predominantly Ca^{2+}-extrusion by NCX) and the derived rate of Serca2a SR Ca^{2+}-uptake in Ctl and pAF models. **C.** Validation of $I_{Ca,L}$ amplitude, CaT amplitude, SR Ca^{2+}-leak and cCaT amplitude (SR Ca^{2+}-load) in Ctl and pAF models. Results were obtained in the absence of spontaneous Ca^{2+}-release events.

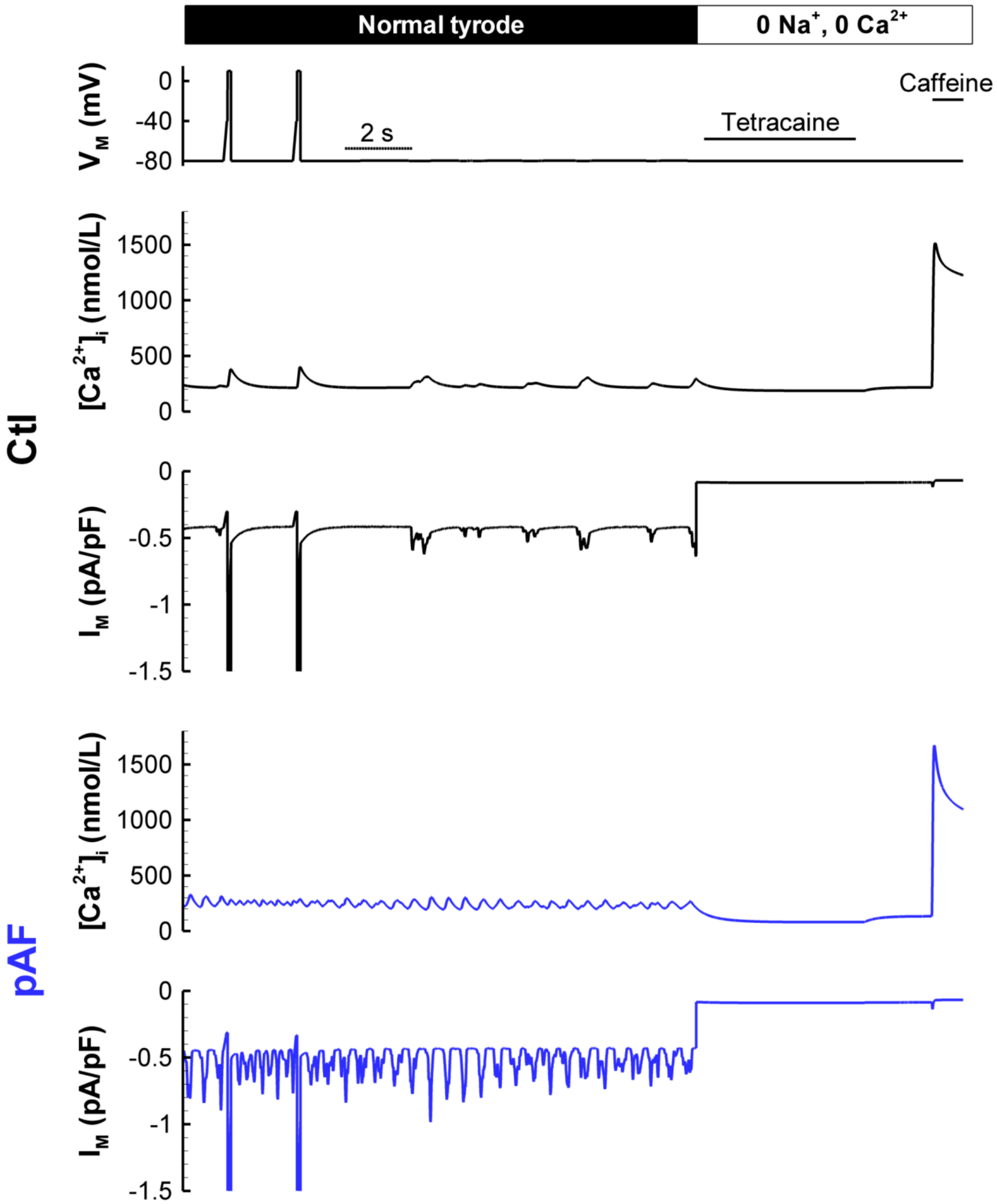

Online Figure VIII. Whole-cell $[Ca^{2+}]_i$ and total membrane current in the control (Ctl) and paroxysmal AF (pAF) models for the simulations shown in **Figure 8**.

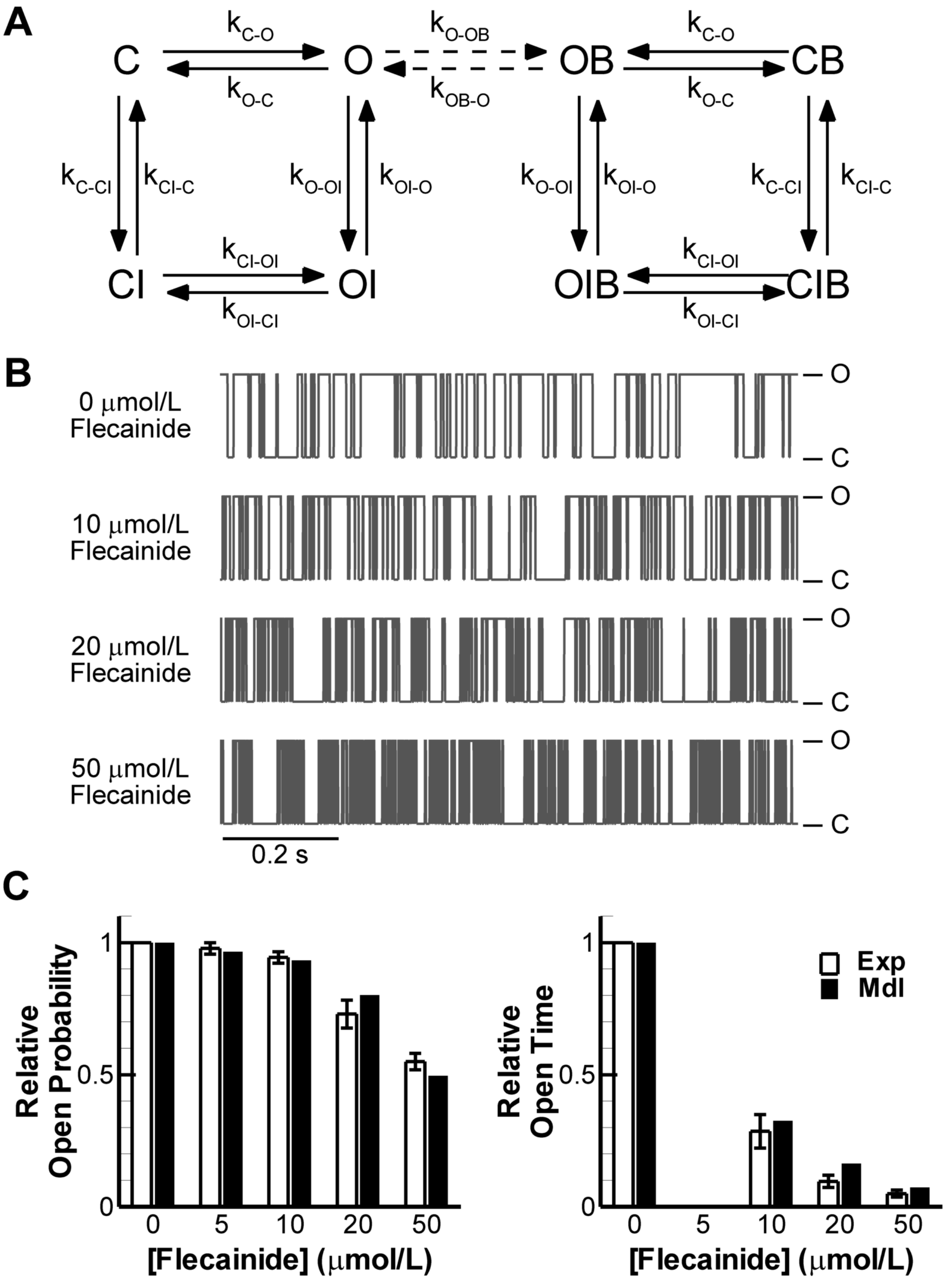

Online Figure IX. Simulation of RyR2 inhibition by flecainide. **A.** RyR2 Markov model structure with group of blocked states accessible via the open state. **B.** Stochastic simulation of single RyR2 at different concentrations of flecainide. **C.** Validation of average RyR2 open probability (left panel) and RyR2 open time (right panel) at increasing concentrations of flecainide in experiments[21] (white bars) and stochastic RyR2 model (black bars).

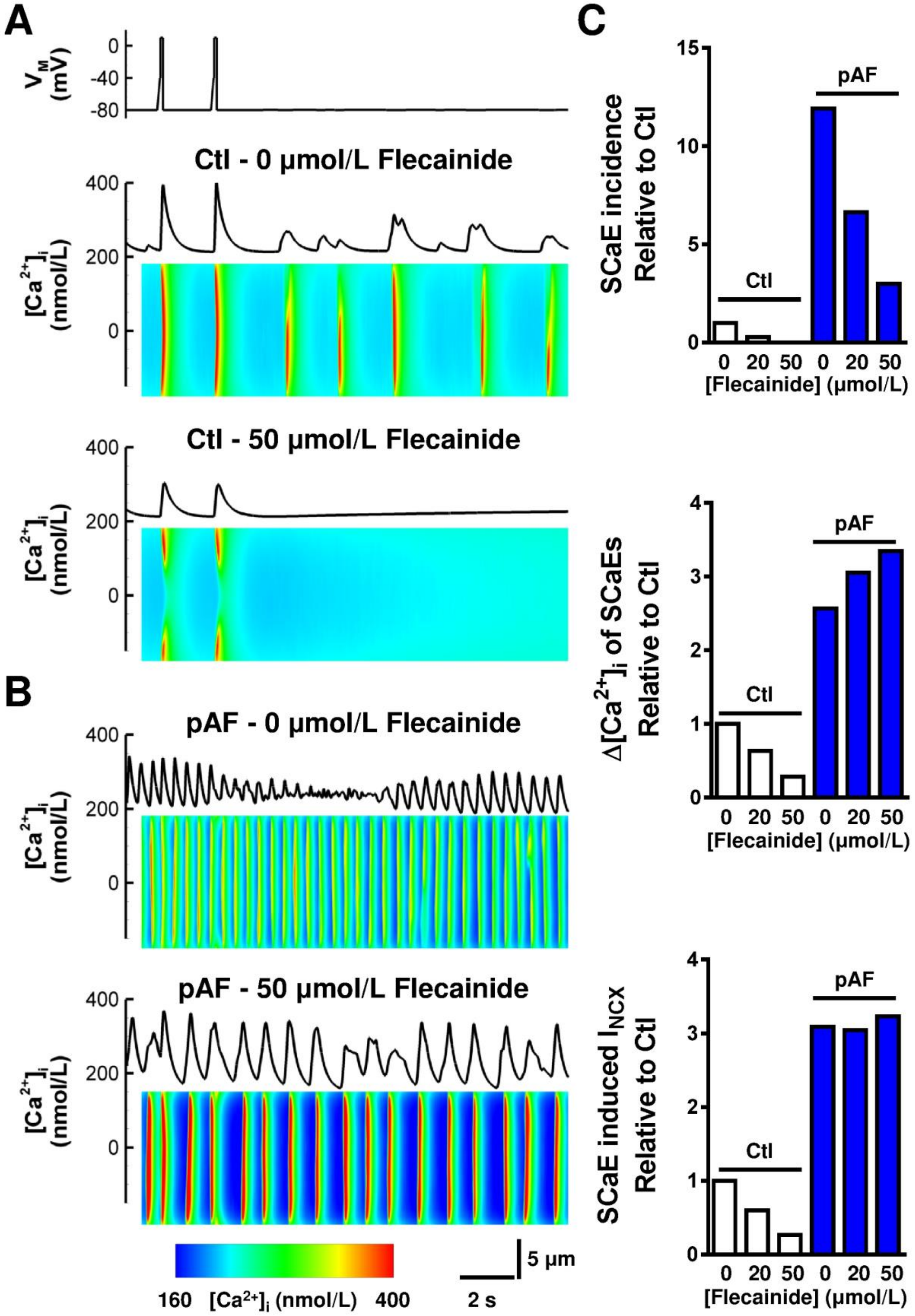

Online Figure X. Effect of simulated flecainide on spontaneous SR Ca^{2+}-release events (SCaEs). **A.** Voltage-clamp protocol, and whole-cell $[Ca^{2+}]_i$ in the absence (top panel) or presence (bottom panel) of 50 µmol/L flecainide in the sinus rhythm control model (Ctl). The insets show a transverse line-scan representation of $[Ca^{2+}]$ at the center of the virtual cell. **B.** Similar to panel A for the paroxysmal AF (pAF) model. **C.** Quantification of the effect of 20 or 50 µmol/L flecainide on SCaE incidence, $\Delta[Ca^{2+}]_i$ (amplitude) of SCaEs, and SCaE-induced membrane current (top to bottom) in Ctl and pAF models.

Flecainide causes a dose-dependent decrease in incidence of SCaEs in both models. In the Ctl model, this is accompanied by a reduction in the amplitude of SCaEs and the corresponding depolarizing membrane inward current. In the pAF model, the reduced incidence of SCaEs in the presence of flecainide allows more time for Ca^{2+}-uptake into the SR, thereby producing lower diastolic $[Ca^{2+}]$ levels, which tend to increase amplitude of SCaEs. The flecainide concentrations employed in our simulations are supratherapeutic, but were necessary to observe an effect due to the relatively low affinity ($IC_{50} \approx 55$ µmol/L) observed in lipid-bilayer experiments when RyR2 channels were activated using high cytosolic $[Ca^{2+}]$,[21] which were used for the parameterization of our model. The differences in the affinity of flecainide towards RyR2 following different activation protocols is at present incompletely understood and therefore not incorporated in our model. We therefore interpret our findings as showing that flecainide concentrations at or below the IC_{50} for RyR2 inhibition can reduce the incidence of SCaEs.

Although the present results suggest that RyR2-inhibition by flecainide has antiarrhythmic properties in pAF, it should be noted that in vivo the effects of flecainide are complex, involving inhibition of Na^+-channels and modulation of intracellular Ca^{2+}-handling via altered intracellular $[Na^+]$, in addition to direct RyR2 inhibition.[22] As such, flecainide may have better antiarrhythmic properties in vivo than suggested by our simulations of RyR2-inhibition alone. On the other hand, it has been shown that Ca^{2+}-overload reduces the efficacy of flecainide against SCaEs,[22] in agreement with our findings that the incidence of SCaEs in the pAF model with flecainide was still greater than in the Ctl model in the absence of flecainide.

Online Videos

Online Video I. Animation of membrane potential, whole-cell Ca^{2+}-transient and spatial $[Ca^{2+}]_i$ distribution over time in the Ctl model. Protocol corresponds to the line-scan image shown in **Figure 8A**, top panel.

Online Video II. Animation of membrane potential, whole-cell Ca^{2+}-transient and spatial $[Ca^{2+}]_i$ distribution over time in the Ctl model with increased SR Ca^{2+}-uptake. Protocol corresponds to the line-scan image shown in **Figure 8A**, second panel.

Online Video III. Animation of membrane potential, whole-cell Ca^{2+}-transient and spatial $[Ca^{2+}]_i$ distribution over time in the Ctl model with RyR2 dysfunction. Protocol corresponds to the line-scan image shown in **Figure 8A**, third panel.

Online Video IV. Animation of membrane potential, whole-cell Ca^{2+}-transient and spatial $[Ca^{2+}]_i$ distribution over time in the pAF model combining increased SR Ca^{2+}-uptake and RyR2 dysfunction. Protocol corresponds to the line-scan image shown in **Figure 8A**, bottom panel.

References

1. Grynkiewicz G, Poenie M, Tsien RY. A new generation of Ca^{2+} indicators with greatly improved fluorescence properties. *J Biol Chem*. 1985;260:3440-3450
2. Varro A, Negretti N, Hester SB, Eisner DA. An estimate of the calcium content of the sarcoplasmic reticulum in rat ventricular myocytes. *Pflugers Arch*. 1993;423:158-160
3. Choi HS, Eisner DA. The role of sarcolemmal Ca^{2+}-ATPase in the regulation of resting calcium concentration in rat ventricular myocytes. *J Physiol*. 1999;515 (Pt 1):109-118
4. Shannon TR, Ginsburg KS, Bers DM. Quantitative assessment of the SR Ca^{2+} leak-load relationship. *Circ Res*. 2002;91:594-600
5. Chelu MG, Sarma S, Sood S, Wang S, van Oort RJ, Skapura DG, Li N, Santonastasi M, Muller FU, Schmitz W, Schotten U, Anderson ME, Valderrabano M, Dobrev D, Wehrens XH. Calmodulin kinase II-mediated sarcoplasmic reticulum Ca^{2+} leak promotes atrial fibrillation in mice. *J Clin Invest*. 2009;119:1940-1951
6. Sood S, Chelu MG, van Oort RJ, Skapura D, Santonastasi M, Dobrev D, Wehrens XH. Intracellular calcium leak due to FKBP12.6 deficiency in mice facilitates the inducibility of atrial fibrillation. *Heart Rhythm*. 2008;5:1047-1054
7. El-Armouche A, Boknik P, Eschenhagen T, Carrier L, Knaut M, Ravens U, Dobrev D. Molecular determinants of altered Ca^{2+} handling in human chronic atrial fibrillation. *Circulation*. 2006;114:670-680
8. Greiser M, Halaszovich CR, Frechen D, Boknik P, Ravens U, Dobrev D, Luckhoff A, Schotten U. Pharmacological evidence for altered src kinase regulation of $I_{Ca,L}$ in patients with chronic atrial fibrillation. *Naunyn Schmiedebergs Arch Pharmacol*. 2007;375:383-392
9. Voigt N, Trausch A, Knaut M, Matschke K, Varro A, Van Wagoner DR, Nattel S, Ravens U, Dobrev D. Left-to-right atrial inward rectifier potassium current gradients in patients with paroxysmal versus chronic atrial fibrillation. *Circ Arrhythm Electrophysiol*. 2010;3:472-480
10. Wehrens XH, Lehnart SE, Huang F, Vest JA, Reiken SR, Mohler PJ, Sun J, Guatimosim S, Song LS, Rosemblit N, D'Armiento JM, Napolitano C, Memmi M, Priori SG, Lederer WJ, Marks AR. FKBP12.6 deficiency and defective calcium release channel (ryanodine receptor) function linked to exercise-induced sudden cardiac death. *Cell*. 2003;113:829-840
11. Grandi E, Pandit SV, Voigt N, Workman AJ, Dobrev D, Jalife J, Bers DM. Human atrial action potential and Ca^{2+} model: sinus rhythm and chronic atrial fibrillation. *Circ Res*. 2011;109:1055-1066
12. Smith PD, Liesegang GW, Berger RL, Czerlinski G, Podolsky RJ. A stopped-flow investigation of calcium ion binding by ethylene glycol bis(beta-aminoethyl ether)-N,N'-tetraacetic acid. *Anal Biochem*. 1984;143:188-195
13. Niggli E. Ryanodine receptors: waking up from refractoriness. *Cardiovasc Res*. 2011;91:563-564

14. Ramay HR, Liu OZ, Sobie EA. Recovery of cardiac calcium release is controlled by sarcoplasmic reticulum refilling and ryanodine receptor sensitivity. *Cardiovasc Res*. 2011;91:598-605

15. Voigt N, Li N, Wang Q, Wang W, Trafford AW, Abu-Taha I, Sun Q, Wieland T, Ravens U, Nattel S, Wehrens XH, Dobrev D. Enhanced sarcoplasmic reticulum Ca^{2+} leak and increased Na^{+}-Ca^{2+} exchanger function underlie delayed afterdepolarizations in patients with chronic atrial fibrillation. *Circulation*. 2012;125:2059-2070

16. Heijman J, Zaza A, Johnson DM, Rudy Y, Peeters RL, Volders PG, Westra RL. Determinants of beat-to-beat variability of repolarization duration in the canine ventricular myocyte: a computational analysis. *PLoS Comput Biol*. 2013;9:e1003202

17. Decker KF, Heijman J, Silva JR, Hund TJ, Rudy Y. Properties and ionic mechanisms of action potential adaptation, restitution, and accommodation in canine epicardium. *Am J Physiol Heart Circ Physiol*. 2009;296:H1017-1026

18. Van Wagoner DR, Pond AL, Lamorgese M, Rossie SS, McCarthy PM, Nerbonne JM. Atrial L-type Ca^{2+} currents and human atrial fibrillation. *Circ Res*. 1999;85:428-436

19. Christ T, Boknik P, Wohrl S, Wettwer E, Graf EM, Bosch RF, Knaut M, Schmitz W, Ravens U, Dobrev D. L-type Ca^{2+} current downregulation in chronic human atrial fibrillation is associated with increased activity of protein phosphatases. *Circulation*. 2004;110:2651-2657

20. Hilliard FA, Steele DS, Laver D, Yang Z, Le Marchand SJ, Chopra N, Piston DW, Huke S, Knollmann BC. Flecainide inhibits arrhythmogenic Ca^{2+} waves by open state block of ryanodine receptor Ca^{2+} release channels and reduction of Ca^{2+} spark mass. *J Mol Cell Cardiol*. 2010;48:293-301

21. Watanabe H, Chopra N, Laver D, Hwang HS, Davies SS, Roach DE, Duff HJ, Roden DM, Wilde AA, Knollmann BC. Flecainide prevents catecholaminergic polymorphic ventricular tachycardia in mice and humans. *Nat Med*. 2009;15:380-383

22. Steele DS, Hwang HS, Knollmann BC. Triple mode of action of flecainide in catecholaminergic polymorphic ventricular tachycardia. *Cardiovasc Res*. 2013;98:326-327